Journal of Hydrology 602 (2021) 126713

Contents lists available at ScienceDirect

Journal of Hydrology

journal homepage: www.elsevier.com/locate/jhydrol

Research papers

Dispersion and recovery of solutes and heat under cyclic radial advection

D.W.S. Tang [*,1], S.E.A.T.M. van der Zee [2]

Soil Physics and Land Management, Wageningen University, Wageningen, the Netherlands

ARTICLE INFO

This manuscript was handled by Corrado Corradini, Editor-in-Chief, with the assistance of William Payton Gardner, Associate Editor

Keywords:
Groundwater
Advection-dispersion
Recovery efficiency
Solute and heat transport
Aquifer Thermal Energy Storage (ATES)
Aquifer Storage and Recovery (ASR)

ABSTRACT

For cyclic injection-extraction wells with various radial flow geometries, we study the transport and recovery of solute and heat. We derive analytical approximations for the recovery efficiency in closed-form elementary functions. The recovery efficiency increases as injection-extraction flow rates increase, dispersion decreases, and spatial dimensionality decreases. In most scenarios, recovery increases as cycle periods increase, but we show numerically and analytically that it varies non-monotonically with cycle period in three-dimensional flow fields, due to competing effects between diffusion and mechanical dispersion. This illustrates essential differences between the spreading mechanisms, and reveals that for a single well it may be impossible to optimize recovery of both solute and heat simultaneously. Whether retardation increases or decreases recovery thus depends on aquifer geometry and the dominant dispersion process. As the dominant dispersion process heavily determines the sensitivity of the recovery efficiency to other parameters, we introduce the dimensionless kinetic dispersion factor S_T, to distinguish whether diffusion or mechanical dispersion dominates. We also introduce the geometric dispersion factor G, which is derived from our full solution for the recovery efficiency and improves upon the concept of the area-to-volume ratio (A/V), often used in analysing well problems. Unlike A/V, G accounts for spatio-temporal interactions between dispersion and flow field geometry, and can be applied to determine recovery efficiencies across a wider range of scenarios. It is found that A/V is a special case of G, describing the recovery efficiency only when mechanical dispersion with linear velocity dependence is the sole mechanism of spreading.

1. Introduction

Wells in geological porous media are used in cyclic injection-extraction processes, otherwise named push–pull processes, in many applications. These include Aquifer Thermal Energy Storage (ATES) (Lee, 2010), Aquifer Storage and Recovery (ASR) (Lowry and Anderson, 2006), subsurface irrigation with excess moisture drainage (Narain-Ford et al., 2020), hydraulic fracturing (Penny et al., 1983), air sparging (van Dijke and van der Zee, 1998), aquifer characterization (Istok et al., 1997; Haggerty et al., 1998; Schroth et al., 2000; Gouze et al., 2008; Anderson, 2005), the treatment of drinking water production aquifers (Van Halem et al., 2011), and gasoline spill remediation (van Dijke and van der Zee, 1998). Natural forces also drive oscillatory environmental flows: coastal aquifers experience oscillatory flows due to tidal, seasonal and glacial cycles, resulting in the oscillatory transport of salinity (Pool et al., 2016) across freshwater lenses. Another example of oscillatory environmental flow is barometric pumping: subsurface gases and vapors are periodically drawn upwards and forced downwards due to seasonal variations in atmospheric pressure (Stauffer et al., 2019; Nilson et al., 1991; Scotter and Raats, 1968). Oscillatory flows also result from a combination of human and natural factors. For example, soils in semi-arid regions receive sodium ions from capillary rise in the dry season, which are subsequently flushed downwards by infiltrating rain and irrigation (van de Craats et al., 2020; van der Zee et al., 2014).

In many of these oscillatory flow problems, an interface separates two bodies of water of different quality, a classical example being the freshwater lens. With aquifer storage systems, the interface separates the injected freshwater or hot water from background groundwater. A chemical or thermal gradient, which undergoes transport due to advection and hydrodynamic dispersion, is responsible for the difference in water quality across the interface. In light of the wide variety of applications, especially regarding water, environmental, and energy sustainability, fundamental research into the general behavior of solute and heat transport under oscillatory conditions has recently received a

* Corresponding author.
E-mail address: darrell.tang@wur.nl (D.W.S. Tang).
[1] ORCID: 0000-0002-4743-3976.
[2] ORCID: 0000-0002-6324-776X.

https://doi.org/10.1016/j.jhydrol.2021.126713
Received 11 May 2021; Received in revised form 6 July 2021; Accepted 16 July 2021
Available online 24 July 2021

significant amount of engagement (e.g. Laemmel et al., 2019; Stauffer et al., 2019; van Duijn and van der Zee, 2018; Dey and Sekhar, 2014; Pauw et al., 2016; Sanz-Prat et al., 2016; Cirkel et al., 2015; Eeman et al., 2017; Wang and Chen, 2015; Lu et al., 2011). Amongst the various oscillatory flow scenarios, managed aquifer recharge systems such as ASR and ATES are unique in that they are concerned with not only the spreading of solutes and heat in the subsurface, but also the recovery of freshwater or heat.

In this study, we characterize the performance of aquifer storage systems. A key performance metric of an injection-extraction system is the recovery efficiency of injected solutes or heat, which is the proportion of injected solute mass or thermal energy that can be recovered during the extraction phase. Solutes and heat spread around the injected water front due to hydrodynamic dispersion processes, that are partly advection velocity-dependent, such as mechanical pore-scale dispersion, and partly velocity-independent, such as molecular and thermal diffusion. The types of dispersion process that occur, the relative strengths of the dispersion processes, the strength of dispersion relative to advection, and a number of other factors such as flow field geometry and injection rate determine the recovery efficiency. We employ analytical methods to derive simple solutions for the recovery efficiency as a function of these parameters, and discuss the implications of well design, well operational parameters, and aquifer characteristics on the recovery efficiency.

2. Literature review

Many prior analytical characterizations of injection-extraction systems make use of exact solutions (e.g. Yang et al., 2010; Yates, 1990; Chen, 1987; Veling, 2012; Aichi and Akitaya, 2018), and are valid for specific scenarios. For example, they might apply only to specific flow field geometries, or omit either mechanical dispersion or molecular diffusion. Some, giving non-closed form functions that require numerical integration, may be somewhat less transparent for directly comparing different geometrical or dispersion properties. Furthermore, no exact analytical solutions are available for some scenarios such as wells modelled as point sources. Quite a number of analytical solutions are available, including studies with closed-form analytical solutions (e.g. Pophillat et al., 2020a; Gelhar and Collins, 1971), but they currently describe only the spatial distribution of concentration and temperature, but not the recovery efficiency. A large body of literature on direct numerical simulations of the recovery efficiency exists, (e.g. Doughty et al., 1982; Sommer et al., 2013; Sommer et al., 2015; van Lopik et al., 2016; Bloemendal and Hartog, 2018; Pophillat et al., 2020a; Pophillat et al., 2020b). However, such numerical studies are computationally intensive and specific to certain combinations of parameter values and aquifer geometry, which makes their findings difficult to generalize. To overcome these limitations, we turn to analytical approximations to describe the recovery efficiency with elementary mathematical functions. Such closed-form analytical approximations allow for straightforward sensitivity analysis, rapid evaluation of a vast parameter space, and identification of suitable regions within parameter space for further in-depth investigation with more exact methods. They also give more insight in synergistic and antagonistic effects of different parameters, and they are fast to evaluate.

The area-to-volume ratio (A/V) is a popular approximate method for estimating the recovery efficiency of radial transport systems (e.g. Sommer et al., 2015; Schout et al., 2014; Novo et al., 2010; Forkel and Daniels, 1995). It is based on a simple principle: in three spatial dimensions "the volume of a storage unit increases as the cube of the characteristic dimension (i.e. storage radius), and its area for heat loss increases as the square, so increasing the size reduces the loss-to-capacity ratio" (Duffie and Beckman, 2013). Similar considerations apply to problems of any number of spatial dimensions. However, the A/V is a purely geometric argument that does not consider other factors within the system, such as those previously described. These other aspects of the system also interact with flow field geometry in determining the recovery efficiency, thus the validity of the A/V ratio in characterizing recovery efficiency hinges upon these other factors. For instance, the evolution of the A/V ratio with time depends on the flow field geometry and injection rate at the well, and so does the Peclet number (Kim et al., 2010). While the A/V ratio might decrease over time as the storage radius increases and indicate a larger recovery efficiency, the magnitude of dispersion relative to advection might in some cases increase with the storage radius thereby suggesting a smaller recovery efficiency. Therefore, the A/V ratio as an indicator of recovery efficiency ignores aspects of complexity that are instrumental to the problem.

Gelhar and Collins' (1971) classical model of concentration profiles around injection wells remains instrumental today in characterizing aquifer-well systems (Pophillat et al., 2020a). Furthermore, Gelhar and Collins' model for the concentration profiles continues to be applied and modified in recent years (e.g. Shi et al., 2020; Guimerà et al., 2007; Schroth and Istok, 2005). Hence, we derive approximate solutions for the recovery efficiency, taking into account the interactions between flow field geometry, hydrodynamic dispersion, and the recovery efficiency, that are ignored with the A/V ratio, by extending the model of Gelhar and Collins (1971), and validating our analytical results with numerical models. For notational convenience and brevity, we proceed with solute transport terminology. Under the assumption that density differences induced by chemical and thermal gradients are negligible, the analysis is mathematically analogous and fully applicable to heat transport (Lee, 1998).

3. Methods

In homogeneous aquifers with negligible background flow, flow fields around wells can be described as radially axisymmetric flow around a point source. Radial flow in one, two, and three dimensions implies a linear, disk-shaped, and spherical flow field, respectively. These three radial geometries correspond respectively to $d = 1, 2, 3$ in the mathematical construct of a d-dimensional sphere. The radially axisymmetric advection–dispersion equation (ADE) describing conservative solute and heat transport in any number of dimensions is (Gelhar and Collins, 1971)

$$\frac{\partial c}{\partial t} = \alpha v \frac{\partial^2 c}{\partial r^2} - v\frac{\partial c}{\partial r} + D_m\left(\frac{\partial^2 c}{\partial r^2} - \frac{1}{v}\frac{\partial v}{\partial r}\frac{\partial c}{\partial r}\right), \tag{1}$$

where r is the radial positional coordinate, c is the dimensionless concentration of the solute, t is time, v is the flow velocity, α is the longitudinal mechanical dispersivity, and D_m is the molecular (or thermal) diffusion coefficient. Chemical and thermal retardation is implicitly considered, as it implies only a linear re-scaling of time.

The pore water velocity $v(r)$, and therefore also the mechanical dispersion, is position-dependent for $d > 1$ in view of mass continuity, where d denotes dimensionality. For d-dimensional axisymmetric radial flow,

$$v(r, d) = \frac{A_d}{r^{d-1}}, \tag{2}$$

$$A_d = \frac{Q}{\theta}\left[\frac{2\pi^{\frac{d}{2}}}{\Gamma\left(\frac{d}{2}\right)}\right]^{-1}, \tag{3}$$

where θ is the porosity, Q is the injection or extraction rate, A_d is the d-dependent shape constant, where the term in square brackets is the surface area of a d-dimensional sphere of unit radius, and Γ is the gamma function. Essentially, (2) and (3) force mass continuity by requiring that the rate of volumetric expansion (contraction) of the body of injected water is equal to the injection (extraction) rate.

In practice, for injection/extraction in groundwater aquifers, the $d = 2$ situation of a fully penetrating well seems to be quite common. The

confining layers below and on top of the aquifer may affect the flow pattern somewhat if they are not completely impermeable. For leaky aquifers or wells that do not penetrate fully, a $d = 3$ point injection may be a more appropriate limiting case. The one-dimensional $d = 1$ case reflects an infinite row of fully penetrating wells, in which case the flow of injected water occurs rectilinearly along one dimension (e.g. Molinari and Peaudeceff, 1977; Sauty, 1977). A graphic illustration of these flow field geometries is presented in Fig. 1. Note that although Fig. 1 illustrates 3D rectangular and cylindrical flow fields for the 1D and 2D cases respectively for the sake of visualization, these cases are identical to 1D line and 2D disk flow fields under the assumption that no dispersion or flow occurs into the confining layers.

Substituting the hydrodynamic dispersion coefficient

$$D(r) = D_m + \alpha v(r), \tag{4}$$

into the ADE (1) allows us to rewrite the ADE in a simpler form:

$$\frac{\partial c}{\partial t} = D(r)\frac{\partial^2 c}{\partial r^2} + \left[(d-1)\frac{D_m}{r} - v(r)\right]\frac{\partial c}{\partial r}. \tag{5}$$

In the base model scenario, at the well, a duration T of injection rate Q alternates with the same duration T of extraction rate $-Q$, in a step-cyclic manner in a d-dimensional infinite domain. We henceforth refer to this base scenario as the standard cycle. The standard cycle consists of equal volumes of injected and extracted water during each phase, $V_{in} = V_{ex}$. Later, we also investigate the effects of varying the ratio of extraction to injection volume. The flow field achieves steady-state instantaneously upon switching between injection or extraction. The well injects a total mass $M = c_0 QT$ of solute, and recovers $M_r(i)$, over the i-th injection period. Therefore, the recoverable proportion F_r of solute over the i-th injection-extraction cycle is

$$F_r(i) = \frac{M_r(i)}{M}. \tag{6}$$

The cumulative solute recovery efficiency after n cycles, F_c, is

$$F_c(n) = \frac{1}{n}\sum_{i=1}^{n}\frac{M_r(i)}{M} = \frac{1}{n}\sum_{i=1}^{n}F_r(i). \tag{7}$$

The initial and boundary conditions that describe this problem are

$$c(r,0) = 0, \tag{8}$$

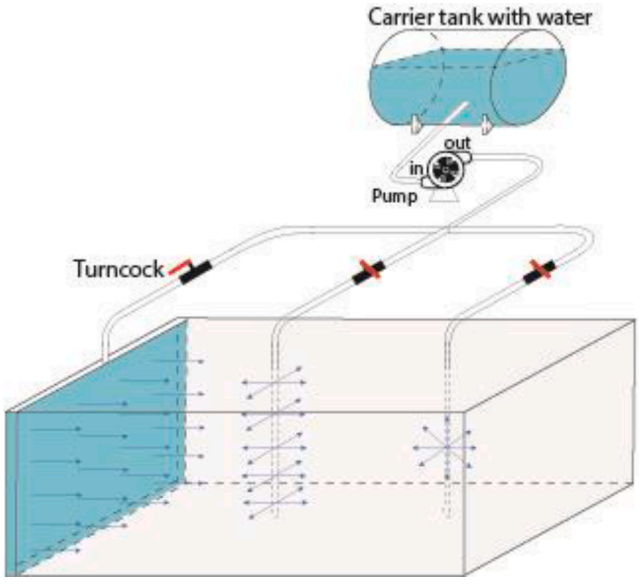

Fig. 1. Conceptual image of (left) 1D, (middle) 2D, and (right) 3D radial flow in a horizontal aquifer.

$$c(0,t)_{in} = c_0, \tag{9}$$

$$\frac{\partial c}{\partial r}(0,t)_{ex} = 0, \tag{10}$$

where subscripts *in* and *ex* refer to the injection and extraction phases respectively. For analytical tractability, we disregard heterogeneity and interactions with the overlying or underlying low hydraulic conductivity layers and flow driven by density gradients, and comment on these simplifications at the end. We also disregard storage periods, where the injection and extraction phases are separated by a period where neither occurs.

Numerical simulations were performed using MODFLOW-2005 (Harbaugh, 2005) and MT3DMS (Langevin and Guo, 2006), for flow and solute transport, respectively. For the computation of the flow field, the initial hydraulic head in the entire domain was set to a uniform value. The boundaries of the numerical domain are set as uniform constant-head boundaries, which imply an absence of background flow. The geometry of the numerical domains are identical to that of the flow field being modelled (i.e. line-, disc-, and sphere-shaped domains for 1D,

Table 1
List of variables. The symbols L, T and M under units represent units of length, time and mass respectively.

Symbol	Units	Description
A_d	$[L^dT^{-1}]$	Shape constant
b	Varies	Placeholder in equation 22
c	$[ML^{-d}]$	Solute concentration
c_0	$[ML^{-d}]$	Injected solute concentration
c_{crit}	$[ML^{-d}]$	Critical solute concentration
d	[–]	Dimensionality
D	$[L^2T^{-1}]$	Hydrodynamic dispersion coefficient
D_m	$[L^2T^{-1}]$	Molecular diffusion coefficient
F_c	[–]	Cumulative recovery efficiency
F_{eff}	[–]	Effective recovery efficiency
F_r	[–]	Recovery efficiency
G	$[L^{xd}T^{y-x}]$	Geometric dispersion factor
i	[–]	i-th cycle
m	[M]	Solute mass lost by the end of the injection phase
m_c	[M]	Solute mass lost by the end of a cycle
M	[M]	Injected solute mass
M_r	[M]	Recovered solute mass
n	[–]	Number of cycles
Q	$[L^dT^{-1}]$	Injection rate
r	[L]	Radial coordinate
r'	[L]	Hydraulic front position
r_m	[L]	Storage radius
S_T	[–]	Kinetic dispersion factor
t	[T]	Time
T	[T]	Injection duration
T_m	[T]	Injection duration that optimizes F_r in 3D flow fields
v	$[LT^{-1}]$	Flow velocity
V	$[L^d]$	Volume of a d-dimensional sphere
V_{in}	$[L^d]$	Injected water volume
V_{ex}	$[L^d]$	Extracted water volume
x	[–]	Exponent for computing F_r and$G$
y	[–]	Exponent for computing F_r and$G$
z	[–]	Exponent for computingF_r
α	[L]	Mechanical dispersivity
Δ	[–]	Placeholder in equation (35)
ζ	Varies	Placeholder in equation (35)
η	[–]	Exponent of power-law mechanical dispersion
θ	[–]	Saturation
ω	[–]	Sub-function for the calculation of concentration profiles

2D, and 3D, respectively). The solute boundary condition at the edge of the domain is

$$\frac{\partial c}{\partial r} = 0, \tag{11}$$

to preserve the continuity of $c(r)$ and minimize dispersive spreading caused by the boundary. To minimize the influence of numerical edge effects on the transport of water and solutes in a semi-infinite domain $0 \le r < \infty$, we placed the boundary sufficiently distant from the source, as checked in pilot simulations. Parameter values used in examples validated with numerical simulations are, unless otherwise specified, $Q = 2^d$, $T = 16$, $\alpha = 0.1$, $D_m = 0.1$, $n = 50$. An overview of the model parameters is presented in Table 1.

$$m(t = T) = \sqrt{\frac{1}{(3d-2)(2d-1)\pi}}(A_d)^{-\frac{3}{2}} Q c_0 \sqrt{(3d-2)\alpha(A_d)^{\frac{3d-1}{d}}(Td)^{\frac{2d-1}{d}} + (2d-1)D_m(A_d)^{\frac{3d-2}{d}}(Td)^{\frac{3d-2}{d}}} \tag{18}$$

4. Theory

4.1. Frontal spreading

The volume of injected water at time t is $V_{in}(t) = Qt$, and the position of the injected water front (i.e. hydraulic front), is given by

$$\begin{aligned} r^{'} &= (dA_d t)^{\frac{1}{d}}, \qquad (t \le T) \\ r^{'} &= (dA_d(2T - t))^{\frac{1}{d}}. \quad (t > T) \end{aligned} \tag{12}$$

where the expression takes on a different form for $t > T$ as injection switches to extraction.

Gelhar and Collins (1971) showed the expression for $c(r, t)$ to be

$$c(r, r^{'}(t)) = \frac{1}{2} c_0 \mathrm{erfc}\left[\frac{r^d - r^{'d}}{dA_d\sqrt{4\alpha\omega}}\right], \tag{13}$$

$$\omega = \int_0^{r^{'}} \frac{v(r) + D_m/\alpha}{v^3(r)} dr. \tag{14}$$

The solution for the concentration during the injection phase $t \le T$, found by substituting (2), (12) and (14) into (13), is

$$c(r, t) = \frac{1}{2} c_0 \mathrm{erfc}\left[\frac{(r^d - (dA_d t))}{\sqrt{4d^2\alpha(dA_d t)^{\frac{2d-1}{d}}}} \sqrt{\frac{(3d-2)(2d-1)\alpha A_d}{(3d-2)\alpha A_d + (2d-1)D_m(dA_d t)^{\frac{d-1}{d}}}}\right] \tag{15}$$

$$F_r(Q, T) = 1 - \left[\sqrt{\frac{2}{(3d-2)(2d-1)\pi}}(A_d)^{-\frac{3}{2}} T^{-1} \sqrt{(3d-2)\alpha(A_d)^{\frac{3d-1}{d}}(Td)^{\frac{2d-1}{d}} + (2d-1)D_m(A_d)^{\frac{3d-2}{d}}(Td)^{\frac{3d-2}{d}}}\right] \tag{21}$$

Expansions of (15) for specific scenarios are given in Table 2.

4.2. Recovery efficiency

The dispersion processes ensure that all solute mass or thermal energy that has escaped beyond the hydraulic front is irrecoverable in a standard cycle. Let m be this irrecoverable solute mass or thermal energy, at the time when the front is at r'. To quantify m outside r' during the injection phase $t \le T$, we integrate the concentration (15) beyond the hydraulic front, as follows:

$$m(t) = \int_{V(r^{'})}^{V(r=\infty)} c(r, t) dV = \int_{r^{'}}^{\infty} c(r, t) \frac{dV(r)}{dr} dr, \tag{16}$$

where $V(r)$ is the volume of a d-dimensional sphere of radius r. Integrating over r the area of a d-dimensional sphere (see Eq. (3)) gives

$$V(r) = \frac{2\pi^{\frac{d}{2}}}{d \cdot \Gamma\left(\frac{d}{2}\right)} r^d \tag{17}$$

Substituting $t = T$ into (16) yields the total solute mass lost at the end of the injection phase:

Let the storage radius

$$r_m = r^{'}(T) = (dA_d T)^{\frac{1}{d}} \tag{19}$$

be the furthest position of the hydraulic front attained during a cycle. Recall that the flow field is modelled as a sequence of successive steady states. Since ω is a path integral over the travel history of the hydraulic front, and since the indefinite integral in ω during the extraction phase is negative of that during the injection phase (Gelhar and Collins, 1971), ω for the complete cycle is:

$$\omega = \int_0^{r_m} \frac{v(r) + D_m/\alpha}{v(r)^3} dr - \int_{r_m}^{0} \frac{v(r) + D_m/\alpha}{v(r)^3} dr = 2\int_0^{r_m} \frac{v(r) + D_m/\alpha}{v(r)^3} dr. \tag{20}$$

Repeating the steps from (13) to (18), and using (20) for ω, yields the total solute mass that disperses out of the hydraulic front by the end of a complete cycle, $m_c = \sqrt{2}m$.

The recovery efficiency over a cycle, which is the ratio of mass not lost to dispersion, to the total solute or thermal mass injected M, is $F_r(Q, T) = 1 - \frac{m_c}{M}$, which yields

Expansions of (21) for specific scenarios are presented in Table 3.

We plotted (21) together with the numerical results for the recovery efficiency of the first cycle in Fig. 2a and b. The solutions agree excellently with the numerical results for all cases, but deviate moderately for 3D flow fields when molecular diffusion dominates at larger T. In this

Table 2
Table of functions describing some limiting cases of transport.

Limiting scenario	Shape constant A_d	Concentration profile $c(r,t)$	Flow exponent x	Period exponent y	Area-to-volume ratio A/V	Geometric dispersion factor $G = Q^x T^y$
1D $D = \alpha\lvert v\rvert$	$A_1 = \frac{Q}{2\theta}$	$\frac{1}{2}c_0\mathrm{erfc}\left[\frac{(r-A_1t)}{\sqrt{4\alpha A_1 t}}\right]$	$-\frac{1}{2}$	$-\frac{1}{2}$	$2\theta(QT)^{-1}$	$Q^{-1/2}T^{-1/2}$
1D $D = D_m$		$\frac{1}{2}c_0\mathrm{erfc}\left[\frac{(r-A_1t)}{\sqrt{4D_m t}}\right]$	-1			$Q^{-1}T^{-1/2}$
1D $D = \alpha\lvert v^2\rvert$		$\frac{1}{2}c_0\mathrm{erfc}\left[\frac{(r-A_1t)}{\sqrt{4\alpha A_1^2 t}}\right]$	0			$T^{-1/2}$
2D $D = \alpha\lvert v\rvert$	$A_2 = \frac{Q}{2\pi\theta}$	$\frac{1}{2}c_0\mathrm{erfc}\left[\frac{(r^2-2A_2t)}{(2A_2t)^{3/4}}\sqrt{\frac{3}{16\alpha}}\right]$	$-\frac{1}{4}$	$-\frac{1}{4}$	$2\sqrt{\pi\theta}(QT)^{-1/2}$	$Q^{-1/4}T^{-1/4}$
2D $D = D_m$		$\frac{1}{2}c_0\mathrm{erfc}\left[\frac{(r^2-2A_2t)}{4A_2t}\sqrt{\frac{A_2}{D_m}}\right]$	$-\frac{1}{2}$	0		$Q^{-1/2}$
2D $D = \alpha\lvert v^2\rvert$		$\frac{1}{2}c_0\mathrm{erfc}\left[\frac{(r^2-(2A_2t))}{\sqrt{16\alpha A_2^2 t}}\right]$	0	$-\frac{1}{2}$		$T^{-1/2}$
3D $D = \alpha\lvert v\rvert$	$A_3 = \frac{Q}{4\pi\theta}$	$\frac{1}{2}c_0\mathrm{erfc}\left[\frac{(r^3-3A_3t)}{(3A_3t)^{5/6}}\sqrt{\frac{5}{36\alpha}}\right]$	$-\frac{1}{6}$	$-\frac{1}{6}$	$3\left(\frac{4\pi\theta}{3}\right)^{\frac{1}{3}}(QT)^{-1/3}$	$Q^{-1/6}T^{-1/6}$
3D $D = D_m$		$\frac{1}{2}c_0\mathrm{erfc}\left[\frac{(r^3-3A_3t)}{(3A_3t)^{7/6}}\sqrt{\frac{7A_3}{36D_m}}\right]$	$-\frac{1}{3}$	$\frac{1}{6}$		$Q^{-1/3}T^{1/6}$
3D $D = \alpha\lvert v^2\rvert$		$\frac{1}{2}c_0\mathrm{erfc}\left[\frac{(r^3-(3A_3t))}{\sqrt{36\alpha A_3^2 t}}\right]$	0	$-\frac{1}{2}$		$T^{-1/2}$

Table 3
Expansions of F_r and S_T for various scenarios.

Scenario	Single cycle recovery efficiency $F_r(Q,T)$	Kinetic dispersion factor S_T
d-dimensions $D = D_m + \alpha\lvert v\rvert$	$1-\left[\sqrt{\frac{2}{(3d-2)(2d-1)\pi}}(A_d)^{-\frac{3}{2}}T^{-1}\sqrt{(3d-2)\alpha(A_d)^{\frac{3d-1}{d}}(Td)^{\frac{2d-1}{d}}+(2d-1)D_m(A_d)^{\frac{3d-2}{d}}(Td)^{\frac{3d-2}{d}}}\right]$	$\frac{(3d-2)\alpha v}{(2d-1)D_m}$
1D $D = D_m + \alpha\lvert v\rvert$	$1-\left[\sqrt{\frac{2}{\pi}}\left(\frac{2\theta}{Q}\right)^{\frac{3}{2}}\sqrt{\alpha\left(\frac{Q}{2\theta}\right)^2T^{-1}+D_m\frac{Q}{2\theta}T^{-1}}\right]$	$\frac{Q\alpha}{2\theta D_m}$
2D $D = D_m + \alpha\lvert v\rvert$	$1-\left[\sqrt{\frac{2}{12\pi}}\left(\frac{2\pi\theta}{Q}\right)^{\frac{3}{2}}\sqrt{2\alpha\left(\frac{Q}{\pi\theta}\right)^{\frac{5}{2}}T^{-1/2}+3D_m\left(\frac{Q}{\pi\theta}\right)^2}\right]$	$\frac{4\alpha}{3D_m}\left(\frac{Q}{4\pi\theta T}\right)^{\frac{1}{2}}$
3D $D = D_m + \alpha\lvert v\rvert$	$1-\left[\sqrt{\frac{2}{35\pi}}\left(\frac{4\pi\theta}{Q}\right)^{\frac{3}{2}}\sqrt{\frac{7}{3}\alpha\left(\frac{3Q}{4\pi\theta}\right)^{\frac{8}{3}}T^{-1/3}+5D_m\left(\frac{3Q}{4\pi\theta}\right)^{\frac{7}{3}}T^{1/3}}\right]$	$\frac{7\alpha}{5D_m}\left(\frac{Q}{36\pi\theta T^2}\right)^{\frac{1}{3}}$
d-dimensions $D = D_m + \alpha\lvert v^2\rvert$	$1-\left[\sqrt{\frac{2}{(3d-2)\pi}}(A_d)^{-\frac{3}{2}}T^{-1}\sqrt{(3d-2)\alpha(A_d)^3T+D_m(A_d)^{\frac{3d-2}{d}}(Td)^{\frac{3d-2}{d}}}\right]$	$\frac{(3d-2)\alpha v^2}{(d)D_m}$
1D $D = D_m + \alpha\lvert v^2\rvert$	$1-\left[\sqrt{\frac{2}{\pi}}\left(\frac{2\theta}{Q}\right)^{\frac{3}{2}}\sqrt{\alpha\left(\frac{Q}{2\theta}\right)^3T^{-1}+D_m\frac{Q}{2\theta}T^{-1}}\right]$	$\frac{Q^2\alpha}{4\theta^2D_m}$
2D $D = D_m + \alpha\lvert v^2\rvert$	$1-\left[\sqrt{\frac{2}{8\pi}}\left(\frac{2\pi\theta}{Q}\right)^{\frac{3}{2}}\sqrt{\alpha\left(\frac{Q}{\pi\theta}\right)^3T^{-1}+4D_m\left(\frac{Q}{\pi\theta}\right)^2}\right]$	$\frac{\alpha}{D_m}\left(\frac{Q}{4\pi\theta T}\right)$
3D $D = D_m + \alpha\lvert v^2\rvert$	$1-\left[\sqrt{\frac{2}{21\pi}}\left(\frac{4\pi\theta}{Q}\right)^{\frac{3}{2}}\sqrt{\frac{7}{9}\alpha\left(\frac{3Q}{4\pi\theta}\right)^3T^{-1}+3D_m\left(\frac{3Q}{4\pi\theta}\right)^{\frac{7}{3}}T^{1/3}}\right]$	$\frac{7\alpha}{3D_m}\left(\frac{Q}{36\pi\theta T^2}\right)^{\frac{2}{3}}$
d-dimensions $D = D_m + \alpha\lvert v^\eta\rvert$	$1-\left[\sqrt{\frac{2}{(3d-2)(3d-2+\eta-\eta d)\pi}}(A_d)^{-\frac{3}{2}}T^{-1}\sqrt{(3d-2)\alpha(A_d)^{\frac{3d-2+\eta}{d}}(Td)^{\frac{3d-2+\eta-\eta d}{d}}+(3d-2+\eta-\eta d)D_m(A_d)^{\frac{3d-2}{d}}(Td)^{\frac{3d-2}{d}}}\right]$	$\frac{(3d-2)\alpha v^\eta}{(3d-2+\eta-\eta d)D_m}$

case, (21) is not a proper expression for F_r, because expression (21) becomes negative at large T, which is physically impossible. This deviation occurs because the approximation (15) is appropriate only when the scale of transport due to hydrodynamic dispersion is not larger than that of advection (Gelhar and Collins, 1971). In 3D, advective transport scales with $r \propto t^{1/3}$ (see Eq. (12)), and thus so does mechanical dispersion. In contrast, displacement due to molecular diffusion scale with $t^{1/2}$ regardless of dimensionality (Woess, 2000). Therefore, (15) and (21) are accurate in all modelled scenarios except in 3D if molecular diffusion is dominant.

Several important characteristics of the system are revealed in (21): F_r increases monotonically as Q increases, and as D decreases. Remarkably, if $\alpha \neq 0$ and $D_m \neq 0$, in 1D and 2D F_r increases monotonically as T increases, but varies non-monotonically in 3D with a maximum. These observations can be explained in further detail, by considering the following scenarios, which we will refer to as limiting scenarios.

Notice that the rightmost root term (21) contains the sum of a mechanical dispersive and a diffusive component. In limiting cases where

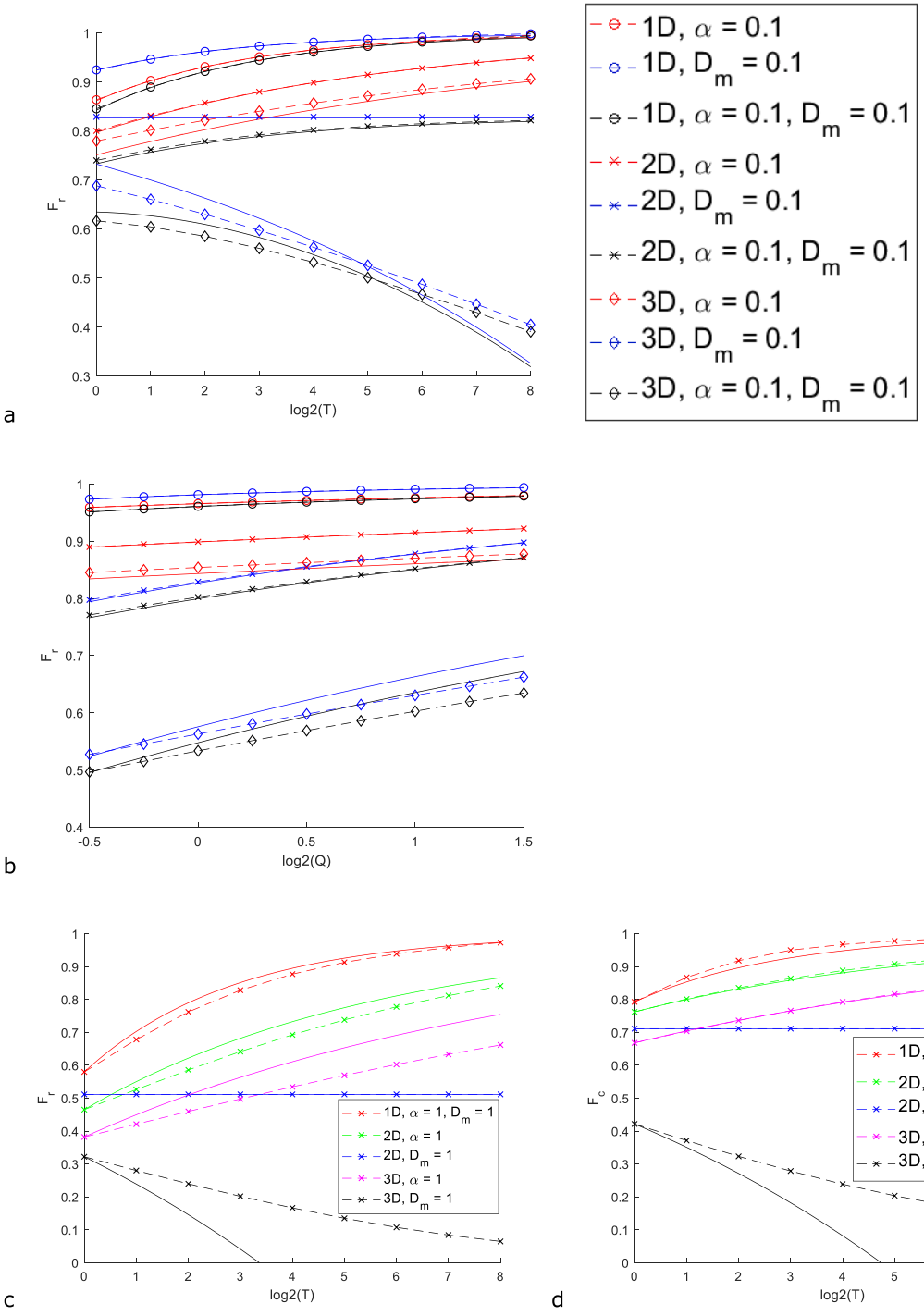

Fig. 2. Dashed lines with markers are numerical results, while solid lines are analytical solutions. (a) First cycle $F_r(T)$ using (21). (b) First cycle $F_r(Q)$ using (21). (c) First cycle $F_r(T)$ extrapolated using (24), (d) $F_c(T)$ after 50 cycles extrapolated using (24). Extrapolations use $T_0 = 1$ as reference.

one hydrodynamic dispersion process completely dominates (i.e. either $D = \alpha|v|$ or $D = D_m$), then (21) simplifies to

$$F_r(Q,T) = 1 - \left[b\sqrt{\alpha}\,|Q^x|T^y\right], \tag{22a}$$

$$x = -\frac{1}{2d}, \tag{22b}$$

$$y = -\frac{1}{2d}, \tag{22c}$$

for $D = \alpha|v|$, and

$$F_r(Q,T) = 1 - \left[b\sqrt{D_m}\,|Q^x|T^y\right], \tag{23a}$$

$$x = -\frac{2}{2d}, \tag{23b}$$

$$y = \frac{d-2}{2d}, \tag{23c}$$

for $D = D_m$, where all terms in (21) not explicitly written in (22a) and (23a) are lumped into b for brevity. Essentially, b is a function of dimensionality, and the identity (but not magnitude) of the dominant

dispersion process. Values of x and y in scenarios of all spatial dimensions are included in Table 2. In all limiting cases, $1-F_r \propto \sqrt{\alpha}$ or $1-F_r \propto \sqrt{D_m}$, regardless of dimensionality. Note however that when both α and D_m are non-zero, the relationship $1-F_r \propto \sqrt{\alpha Q + D_m}$ does not hold. As follows from the above equations, the period exponent y and flow exponent x are crucial in determining how both concentration profile and dispersive loss are affected by T and Q. In the limiting cases described by (22)–(23), $F_r(d=2, D=D_m)$ is independent of T, and $F_r(d=3, D=D_m)$ decreases as T increases. In all other limiting cases, F_r increases as T increases and as Q increases. The fact that $F_r(d=3, D=D_m)$ decreases as T increases, whereas $F_r(d=3, D=\alpha|v|)$ increases as T increases, explains why $F_r(d=3, D=\alpha|v|+D_m)$ varies non-monotonically with T. Many problems in practice can be reduced to such limiting cases. For example, thermal diffusion typically dominates heat transport (Anderson, 2005; Vandenbohede et al., 2009), while mechanical dispersion typically dominates solute transport (Anderson, 1984).

Direct estimation with (21) is inaccurate if the hydrodynamic dispersion coefficient is sufficiently large to result in a single cycle F_r smaller than 0.7. The reason is that in scenarios with smaller F_r, the scale of dispersive transport becomes large relative to advection. Nevertheless, in practice aquifer storage systems typically have recovery efficiencies of 0.7 or higher (Drijver et al., 2012) except for systems with very large concentration or thermal gradients where density effects play a significant role in transport (Schout et al., 2016), thus (21) remains applicable to real systems. (21) is also inaccurate in predicting the cumulative recovery efficiency F_c if the number of cycles is larger than 1. In these two cases, it is possible to gain insight on $F_r(Q,T)$ and the cumulative recovery efficiency $F_c(Q,T)$ by extrapolation, even if α and D_m are unknown, provided it is a limiting case where either mechanical dispersion or molecular diffusion completely dominates. If $F_r(Q_0,T_0)$ or $F_c(Q_0,T_0)$ of some reference injection rate Q_0 and injection period T_0 is known, then the recovery efficiency for any Q,T can be approximated using

$$F_r(Q,T) = 1-[1-F_r(Q_0,T_0)]\left(\frac{Q}{Q_0}\right)^x\left(\frac{T}{T_0}\right)^y. \tag{24a}$$

$$F_c(Q,T) = 1-[1-F_c(Q_0,T_0)]\left(\frac{Q}{Q_0}\right)^x\left(\frac{T}{T_0}\right)^y. \tag{24b}$$

Fig. 2c shows a good agreement for the single cycle recovery efficiency F_r, and Fig. 2d for the cumulative recovery efficiency F_c after 50 cycles. A comparison of Fig. 2c and d suggests that the accuracy of the extrapolation improves as the number of elapsed cycles increases. Here too, the solution is inaccurate in 3D scenarios where molecular diffusion dominate, but (24) nevertheless reveals the qualitatively valid outcome that F_r decreases as T increases.

A retardation factor representing linear adsorption implies a linear re-scaling of time. Thus, for a fixed injection duration T, an increase in the retardation factor implies a decrease in recovery for scenarios where $y<0$, and vice versa. This means that the linear retardation of diffusion-dominated transport hinders recovery in 1D flow fields, has no effect in 2D flow fields, and enhances recovery in 3D flow fields.

4.3. Multiple cycles

Consider a scenario in which the total operational duration of the injection-extraction well is prescribed, whereas the total number of cycles N is a variable. Assume that one standard cycle operated with an injection duration of T_0 results in a total solute mass loss of $m_c(T=T_0, N=1)=m_{0,0}$. In the low frequency multiple cycle scenario ($T=nT_0$, $N=1$), where $n>1$ is an arbitrary integer, the total solute mass loss is $m_{n,0}=n^y m_{0,0}$. The high frequency multiple cycle case is ($T=T_0, N=n$), and has an identical total duration as the low frequency multiple cycle case. We approach the high frequency case by first assuming that $m_{0,n}=(n)^z m_{0,0}$, where z is a constant. Then, the upper bound of the cycle exponent z can be inferred by assuming that $c(r)=0$ at the onset of each new cycle, whereupon $m_{0,n}=nm_{0,0}$ exactly, and $z=1$. If this assump-

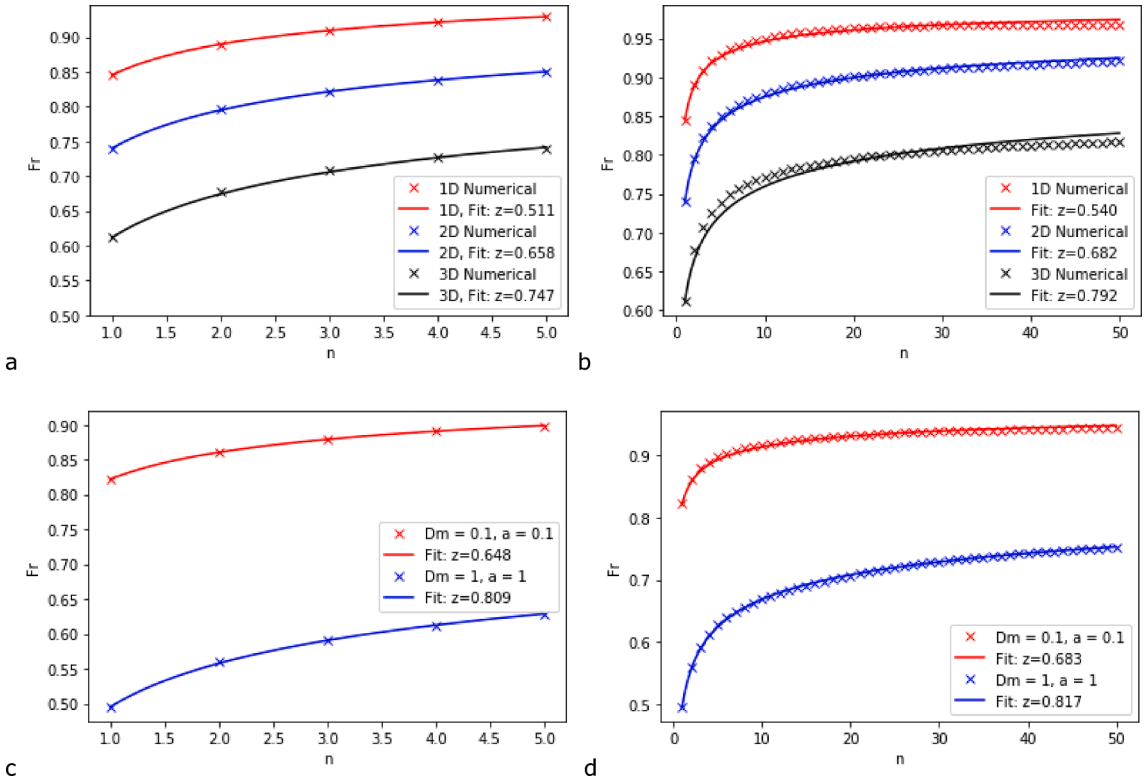

Fig. 3. Recovery efficiency F_r as a function of the n-th cycle, fitted to (25) after (a,c) 5 cycles and (b,d) 50 cycles, showing the effect of (a,b) spatial dimensionality and (c,d) dispersion parameters in a 2D scenario.

tion is omitted, then $m_{0,n} < (n)^z m_{0,0}$, thus we can conclude $z < 1$.

A lower bound for z is found if after the first injection phase, the boundary condition at the well is $\left(\frac{\partial c}{\partial r}(0,t) = 0\right)$ instead of $(c(0,t) = c_0)$, so that previously extracted water is re-injected, without mixing in the well. In this case, multiplying the number of cycles by n implies that ω is also multiplied by n, which yields $m_{0,n} = \sqrt{n} m_{0,0}$, or $z = 1/2$. Under the original boundary condition $(c(0,t) = c_0)$, new solute is injected into the system, therefore $z > 1/2$ necessarily.

In summary, we have found for the cycle exponent that $\frac{1}{2} < z \leq 1$. Using $m_{0,n} = n^z m_{0,0}$, we obtain the recovery efficiency of the n-th cycle

$$F_r(h) = 1 - \frac{m_{0,0} n^z}{M_{0,0} n} = 1 - \left(1 - F_{r,0}\right) n^{z-1}, \tag{25}$$

where $F_{r,0}$ is the recovery efficiency of the first cycle. Numerical results using empirically fitted z agree excellently with (25) (Fig. 3), and fitted z values fall within the bounds predicted $\frac{1}{2} \leq z \leq 1$. Fig. 3 also shows that although the fitted value of z increases slightly with the number of cycles, the difference is small even when data from 5 and 50 cycles is compared. This shows the added value that only a minimal amount of data is required to empirically calibrate z.

The manner by which the upper and lower bounds for the cycle exponent z have been derived, suggest that z can be interpreted as a measure of how much the recovery efficiency of a cycle is affected by all preceding cycles. The larger the value of z, the smaller this memory effect. Fig. 3a,b illustrates this, showing that z increases as the spatial dimensionality increases. This occurs because in each subsequent cycle, the ambient chemical gradient enveloping the new injection water front dissipates more rapidly when the spatial dimensionality is large, thus weakening the memory effect. Similarly, Fig. 3c,d shows that a larger dispersion coefficient $D = D_m + \alpha v$ leads to faster dissipation of ambient solute, resulting in a larger z. Comparing all the scenarios shown in Fig. 3 reveals that z is inversely related to F_r of the first cycle; this is logical in that a complete recovery implies no memory effect, and vice-versa.

Combining (24) and (25), $F_r(Q,T,n)$ can be extrapolated from a reference operation with known $F_r(Q_0,T_0,n_0)$, by using

$$F_r(Q,T,n) = 1 - \left[1 - F_r(Q_0,T_0,n_0)\right] \left(\frac{Q}{Q_0}\right)^x \left(\frac{T}{T_0}\right)^y \left(\frac{n}{n_0}\right)^{z-1}. \tag{26}$$

From (26), we can deduce how cycle frequency affects dispersive losses. If $y > z-1$, then high frequency operations under a prescribed total time result in larger F_r, and vice-versa. Since $z > 1/2$, it means that in 1D where $y = 1/2$, more dispersive losses occur for high than for low frequencies (Fig. 4a). Since $z \leq 1$, it follows that for $y \geq 1$, more dispersive losses occur in low than for high frequencies. Therefore, for $D = D_m$ in 2D $(y = 1)$ (Fig. 4b) and 3D $(y = 7/6)$ (Fig. 4c), F_c decreases as T increases in the case of a fixed total time. This is in contrast with the case of $D = D_m$ for a fixed T, where F_c is independent of T in 2D, and decreases as T increases in 3D. If $y \approx z-1$, then recovery is roughly independent of frequency; this is most likely to occur in general in 2D, where $-\frac{1}{4} \leq y \leq 0$ and $-\frac{1}{2} \leq z-1 \leq 0$, and the ranges of y and $z-1$ overlap closely (e.g. curves for $D = \alpha|v|$ in Fig. 4b).

4.4. Kinetic dispersion factor

In $d = 1$, the velocity and hence hydrodynamic dispersion coefficient is the same everywhere. For $d > 1$, since $R \propto T^{1/d}$, the cycle period influences the relative lengths of time for which dispersive loss is primarily controlled by either mechanical dispersion or molecular diffusion. The relative contribution from mechanical dispersion $\alpha|v|$ to the dispersion coefficient $D = D_m + \alpha|v|$ decreases with R and $T^{1/d}$ as distance increases, because $|v|$ decreases with distance. Therefore, in $d > 1$, the dominant process of spreading of solutes around the plume front increasingly shifts towards molecular diffusion, with distance from the well. Field evidence has shown that thermal breakthrough curves are highly sensitive to mechanical dispersivity at early times of the injection phase, due to the large $v(R)$ associated with small plume volumes (Vandenbohede et al., 2011). This means that some ATES systems are controlled by mechanical disperson (Lin et al., 2019) although heat transport is predominantly controlled by thermal diffusion in uniform flow fields. Hence, it is

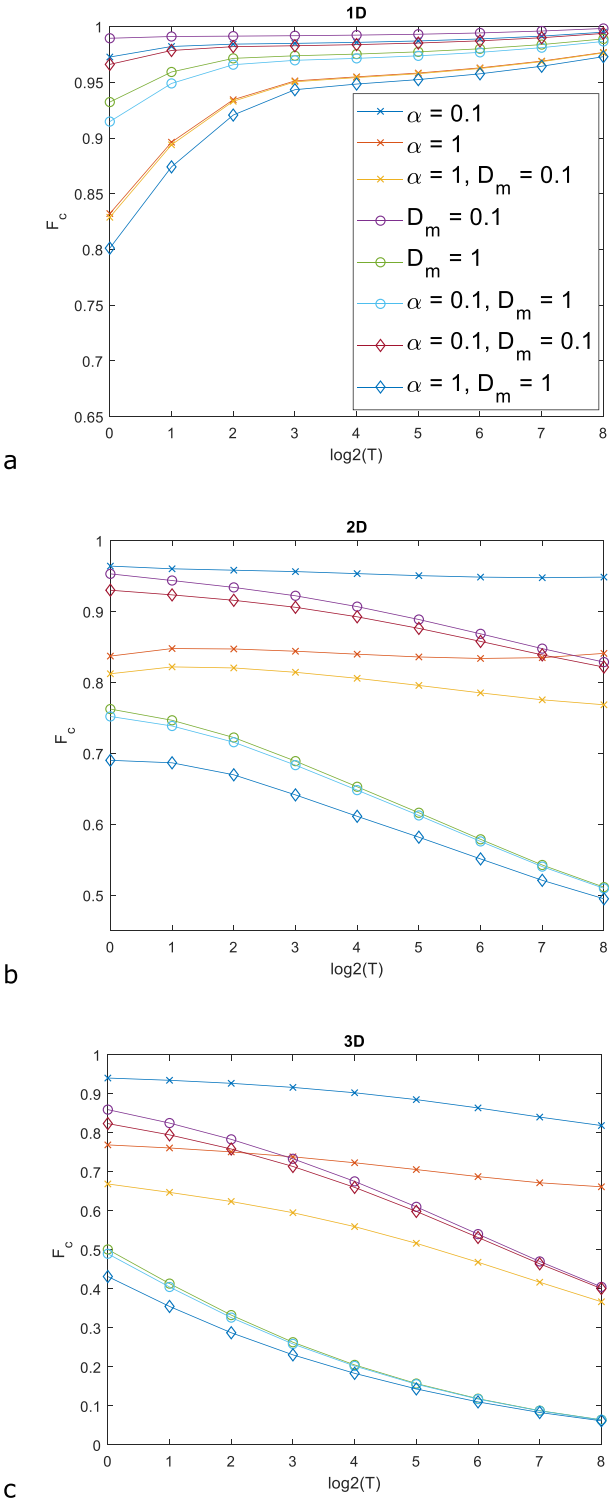

Fig. 4. Numerical results for the variation of the cumulative recovery efficiency F_c against cycle period for fixed total time with $2nT = 512$ after 50 cycles, in a (a) 1D, (b) 2D, and (c) 3D homogeneous medium.

important to be able to determine the relative strengths of diffusion and mechanical dispersion as a function of well operational parameters.

Dispersive losses attributable to $\alpha|v|$, relative to D_m, can be obtained by taking the ratio of their contributions to F_r in (21), and yields

$$\sqrt{S_T} = \sqrt{\frac{(3d-2)\alpha(A_d)^{\frac{3d-1}{d}}(Td)^{\frac{2d-1}{d}}}{(2d-1)D_m(A_d)^{\frac{3d-2}{d}}(Td)^{\frac{3d-2}{d}}}}. \tag{27}$$

where we introduce the dimensionless kinetic dispersion factor S_T. Writing this in terms of $v(R)$ yields

$$S_T = \frac{(3d-2)\alpha v(R)}{(2d-1)D_m}. \tag{28}$$

which is a weighted form of the ratio $\frac{\alpha v(R)}{D_m}$ of the components of $D(r) = D_m + \alpha v(R)$. The unweighted ratio omits the contribution of the term $(d-1)\frac{D_m}{r}\frac{\partial c}{\partial r}$ to the ADE (5). In 1D, $(d-1)\frac{D_m}{r}\frac{\partial c}{\partial r}$ vanishes and the weighted ratio becomes equal to the unweighted ratio. As spatial dimensionality increases, so does S_T, which suggests that the effects of velocity-dependent and velocity-independent dispersion are increasingly different in higher dimensional spaces. Expansions of S_T are presented in Table 3. Concepts similar to S_T have been used in prior studies to determine relative contributions of the dispersion processes in radial flow. Hoopes and Harleman (1967) obtained a weighted ratio, $\frac{4\alpha v(R)}{3D_m}$, which is (28) with $d = 2$ specifically, while Bloemendal and Hartog (2018) applied the unweighted ratio $\alpha v(R)/D_m$ to a two-dimensional radial problem, which underestimates the contribution of mechanical dispersion.

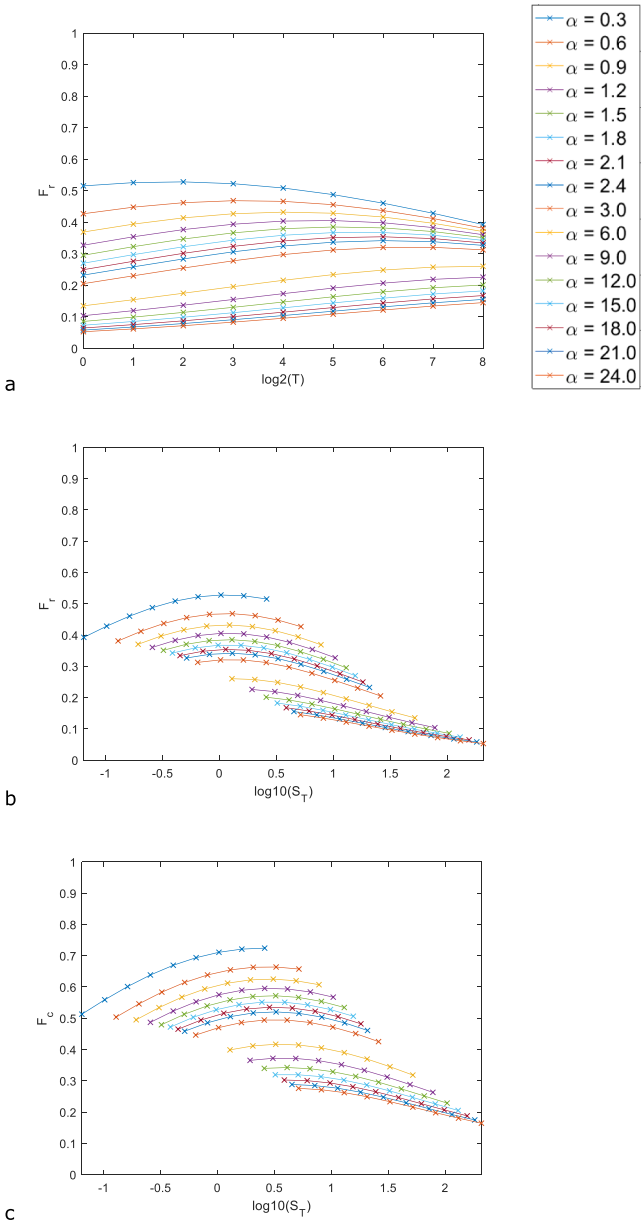

Fig. 5. The relationship between (a) T and F_r for the first cycle, (b) S_T and F_r for the first cycle, and (c) S_T and F_c after 50 cycles, for 3D injection-extraction from a point source; $D_m = 0.1$.

In 3D scenarios, $F_r(T)$ increases monotonically for $D = \alpha|v|$, yet decreases monotonically for $D = D_m$. Thus, a logical reason for the non-monotonicity of $F_r(T)$ in 3D (Fig. 5a) is that the relative strengths of $\alpha|v|$ and D_m at the hydraulic front change with T. Solving $\frac{\partial F_r(T)}{\partial T} = 0$ in (21) yields $S_T = 1$; this agrees with the numerical results for F_r (Fig. 5b). Therefore, the optimum period T_m that corresponds to the maximum $F_r(T)$ can be found by solving substituting $T = T_m$, $d = 3$, and $S_T = 1$ in (27), and solving for T_m:

$$T_m = \sqrt{\left(\frac{7\alpha}{5D_m}\right)^3 \frac{Q}{36\pi\theta}}. \tag{29}$$

(29) agrees excellently with numerical results for the first cycle (Fig. 6). Empirically, we observe that F_c after 50 cycles also peaks close to $S_T = 1$ (Fig. 5c). However, the presence of ambient solute in the aquifer causes (29) to overestimate T_m for multiple cycles (Fig. 6), as only the first cycle recovery efficiency was considered in deriving (29).

Nevertheless, Fig. 6 shows that the proportional relationship $T_m \propto \left(\frac{\alpha}{D_m}\right)^{3/2}$ remains valid even after 50 cycles.

4.5. Geometric dispersion factor

Recall that $A_d \propto Q$. The area-to-volume ratio (A/V), which was previously discussed in the introduction, is

$$\frac{A}{V} = \frac{d}{(dA_dT)^{\frac{1}{d}}} \propto (QT)^{-\frac{1}{d}}, \tag{30}$$

which suggests that either Q or T should be maximized, to minimize losses through the surface area.

While A/V is identical for any combination of Q and T that yield identical QT, the recovery efficiency can significantly differ for different combinations of Q and T. Doughty et al (1982) found that when the total solute mass injected c_0QT was kept constant, in a system with $D = D_m$, the recovery efficiency was higher under large Q small T operation, than under small Q large T operation. Bloemendal and Hartog (2018) investigated heat storage in a system with a 2D flow field. They concluded from sensitivity analyses of Q that $1 - F_r \propto A/V$ approximately when thermal diffusion dominates, which agrees superficially with our findings for 2D flow fields that $1 - F_r \propto Q^{-\frac{1}{2}}T^0$ (Equation 23), because $A/V \propto (QT)^{-\frac{1}{2}}$. Since T was not tested, framing the solution in terms of A/V might lead to ambiguity in interpretation. The principle behind A/V does not consider that the rate of velocity dependent and independent dispersive loss depend differently on plume area and volume, and flow field dimensionality.

The recovery efficiency can be expressed as a function of Q and T in the limiting cases previously discussed where a single dispersion process dominates, namely $1 - F_r \propto Q^x T^y$ (22 – 23), which is similar in form to $A/V \propto (QT)^{-\frac{1}{d}}$. Therefore, as an alternative to A/V, we propose the geometric dispersion factor G:

$$G = Q^x T^y, \tag{31}$$

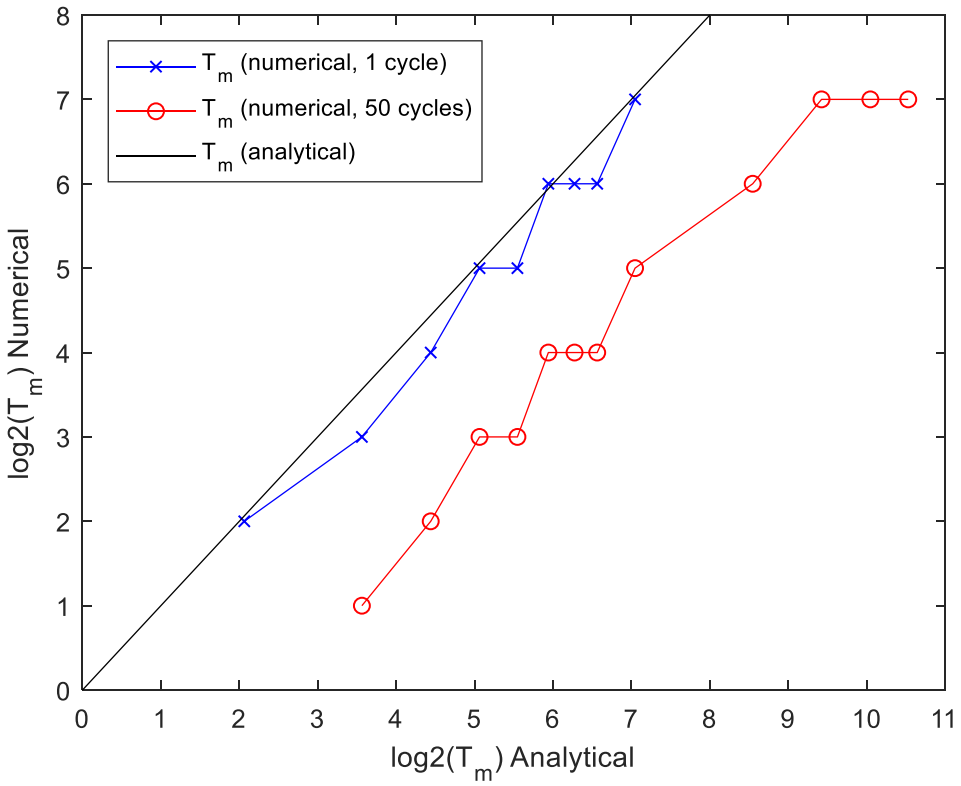

Fig. 6. The numerically obtained and analytically approximated (Eq. (35)) optimum cycle period T_m, corresponding to (crosses) maximum F_r for the first 1 cycle, and (circles) maximum F_c after 50 cycles.

The curves in Fig. 2a and b for scenarios with a single dominant dispersion process illustrate the dependence of G on T and Q respectively. Unlike A/V, the exponents of Q and T in G are not necessarily identical. Essentially, G generalizes A/V, by considering spatio-temporal (as opposed to solely spatial) interactions between plume geometry and hydrodynamic dispersion. Table 2 shows that G is a function of A/V, namely $G \propto \sqrt{A/V}$, only when the velocity-independent dispersion process is omitted. Hence, G should replace A/V in the characterization of aquifer-well systems, as it provides deeper insight into how recovery varies with well operation parameters.

4.6. Production and recovery

By substituting (12) into (13), and using the form of ω appropriate for the extraction phase (Gelhar and Collins, 1971),

$$\omega = \int_0^{r_m} \frac{v(r) + D_m/\alpha}{v(r)^3} dr + \int_{r_m}^{r} \frac{v(r) + D_m/\alpha}{-v(r)^3} dr \tag{32}$$

the production concentration or temperature at the well during the extraction phase $c(r = 0, t > T)$ is found to be

$$c = \frac{1}{2} c_0 \mathrm{erfc}\left[\frac{-[2T - t]}{\sqrt{4d^2\alpha}} \sqrt{\frac{(3d-2)(2d-1)\alpha A_d}{(3d-2)\alpha A_d (dA_d)^{\frac{-1}{d}} \left\{ 2T^{\frac{2d-1}{d}} - [2T-t]^{\frac{2d-1}{d}} \right\} + (2d-1) D_m (dA_d)^{\frac{d-2}{d}} \left\{ 2T^{\frac{3d-2}{d}} - [2T-t]^{\frac{3d-2}{d}} \right\}}} \right] \tag{33}$$

In order to analyze the production concentration and recovery efficiency in non-standard cycles where $\frac{V_{ex}}{V_{in}} \neq 1$ we seek to express (33) as a function of $V_{in} = QT$ and $V_{ex} = Q \cdot (t - T)$, where Q in (33) originates from A_d. This yields, for limiting case where $D = \alpha v$,

$$c(r = 0, t > T) = \frac{1}{2} c_0 \mathrm{erfc}\left[\left(\frac{V_{ex}}{V_{in}} - 1 \right) \left[\frac{V_{in} \Gamma\left(\frac{d}{2}\right) d}{2\theta \pi^{\frac{d}{2}}} \right]^{\frac{1}{2d}} \sqrt{\frac{(2d-1)}{4d^2\alpha \left[2 - \left| 1 - \frac{V_{ex}}{V_{in}} \right|^{\frac{d-1}{d}} \left(1 - \frac{V_{ex}}{V_{in}} \right) \right]}} \right] \tag{34a}$$

where the absolute function ensures that $c(r = 0, t > T)$ remains real and continuous for $V_{ex} \geq V_{in}$. For the opposite limiting case, when $D = D_m$,

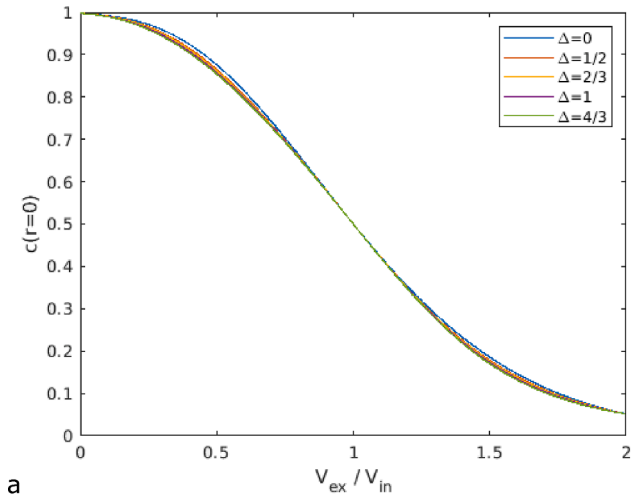

a

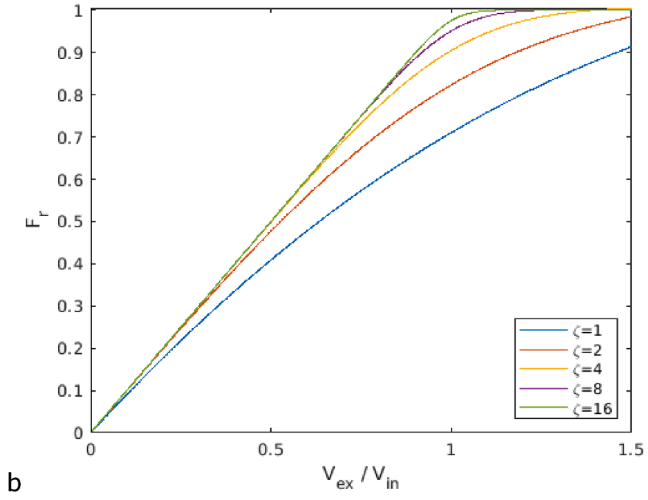

b

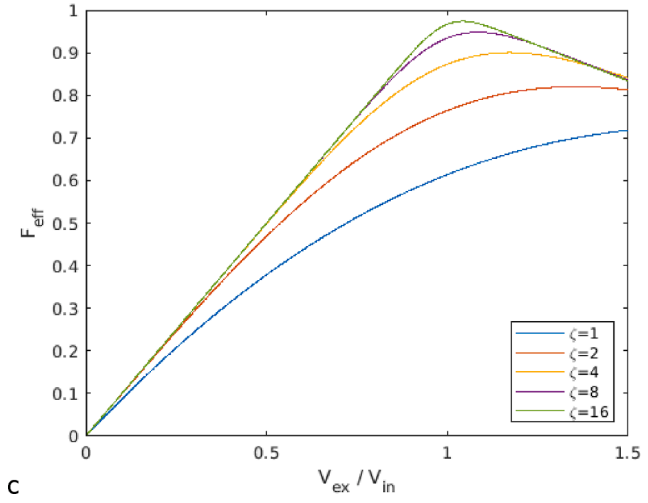

c

Fig. 7. (a) Production concentration $c(r=0)$ against the extraction ratio $\frac{V_{ex}}{V_{in}}$ when $\zeta = 2$. (b) Recovery efficiency F_r against $\frac{V_{ex}}{V_{in}}$, for $\Delta = \frac{1}{2}$. (c) Effective recovery efficiency F_{eff} against $\frac{V_{ex}}{V_{in}}$ for $c_{crit} = \frac{1}{4}c_0$.

$$(r=0, t>T) = \frac{1}{2}c_0 \mathrm{erfc}\left[\left(\frac{V_{ex}}{V_{in}} - 1\right)\left[\frac{V_{in}\Gamma\left(\frac{d}{2}\right)d}{2\theta\pi^{\frac{d}{2}}}\right]^{\frac{2-d}{2d}} \sqrt{\frac{(3d-2)A_d}{4d^2 D_m\left\{2 - \left|1-\frac{V_{ex}}{V_{in}}\right|^{\frac{2d-2}{d}}\left(1-\frac{V_{ex}}{V_{in}}\right)\right\}}}\right] \quad (34b)$$

We can rewrite the production concentrations of the two limiting cases (34) in the form

$$c\left(r=0, \frac{V_{ex}}{V_{in}}\right) = \frac{1}{2}c_0 \mathrm{erfc}\left[\zeta \frac{\left(\frac{V_{ex}}{V_{in}} - 1\right)}{\sqrt{\left\{2 - \left|1-\frac{V_{ex}}{V_{in}}\right|^{\Delta}\left(1-\frac{V_{ex}}{V_{in}}\right)\right\}}}\right], \quad (35)$$

where the exponent Δ ranges from $0 \le \Delta \le \frac{4}{3}$ depending on the spatial dimensionality and dominant hydrodynamic dispersion process, and the other terms are lumped into the constant ζ for readability. Fig. 7a shows that for a fixed value of ζ, the influence of varying the exponent Δ on the production concentration is negligible. Therefore, $\frac{V_{ex}}{V_{in}}$ is effectively the only independent variable in (35) if ζ is fixed. Physically, this implies that at any given production concentration, the marginal effect on the production concentration of increasing $\frac{V_{ex}}{V_{in}}$ is almost independent of flow field dimensionality and the dominant hydrodynamic dispersion process. Therefore, the recovery efficiency as a function of $\frac{V_{ex}}{V_{in}}$ can be obtained by numerically integrating (35) with respect to $\frac{V_{ex}}{V_{in}}$, the outcomes of which for $\Delta = \frac{1}{2}$ are shown in Fig. 7b.

The concavity of the curves in Fig. 7b implies that the marginal benefit to F_r of increasing $\frac{V_{ex}}{V_{in}}$, has diminishing returns in all cases. Where ζ is small (e.g. 3D scenarios, or scenarios with large D), F_r of a symmetric cycle $\frac{V_{ex}}{V_{in}} = 1$ is small. In these cases, using a longer extraction period $\frac{V_{ex}}{V_{in}} > 1$ can increase F_r significantly (Fig. 7b), because there remains relatively large amounts of solute mass deposited immediately outside the hydraulic front. However, where ζ is large, the marginal benefit to F_r is small when $\frac{V_{ex}}{V_{in}}$ is increased beyond 1. This agrees with Sauty et al's (1982) conclusion that symmetric cycles yield an optimum balance between cost (V_{ex}) and benefit (F_r).

In some applications, the recovered hot water in ATES is too cold for heating, or in ASR is of marginal quality for drinking or irrigation, if the production concentration or temperature falls below a critical value c_{crit}. Hence, we may define the effective recovery efficiency as

$$F_{eff} = \frac{\int [c(r=0) - c_{crit}]\, dV_{ex}}{(c_0 - c_{crit})V_{in}}. \quad (36)$$

An example F_{eff} as a function of $\frac{V_{ex}}{V_{in}}$, solved numerically, is presented in Fig. 7c, with $\Delta = \frac{1}{2}$ and $c_{crit} = \frac{1}{4}c_0$. If $\frac{V_{ex}}{V_{in}} = 1$, then F_{eff} is simply equal to $\frac{F_r - (c_{crit}/c_0)}{1-(c_{crit}/c_0)}$. Once $c(r=0, t>T) < c_{crit}$, extraction should cease, because the remaining water is unusable and the marginal benefit of increasing $\frac{V_{ex}}{V_{in}}$ becomes negative. Extraction of additional water beyond this point will degrade the quality of the earlier extracted water, if they mix. The marginal benefit to F_{eff}, of increasing $\frac{V_{ex}}{V_{in}}$, becomes smaller for larger c_{crit}, because $[c(r=0) - c_{crit}]$ monotonically decreases as c_{crit} increases. These diminishing returns can become negative returns if c_{crit} is non-zero, as illustrated in Fig. 7c.

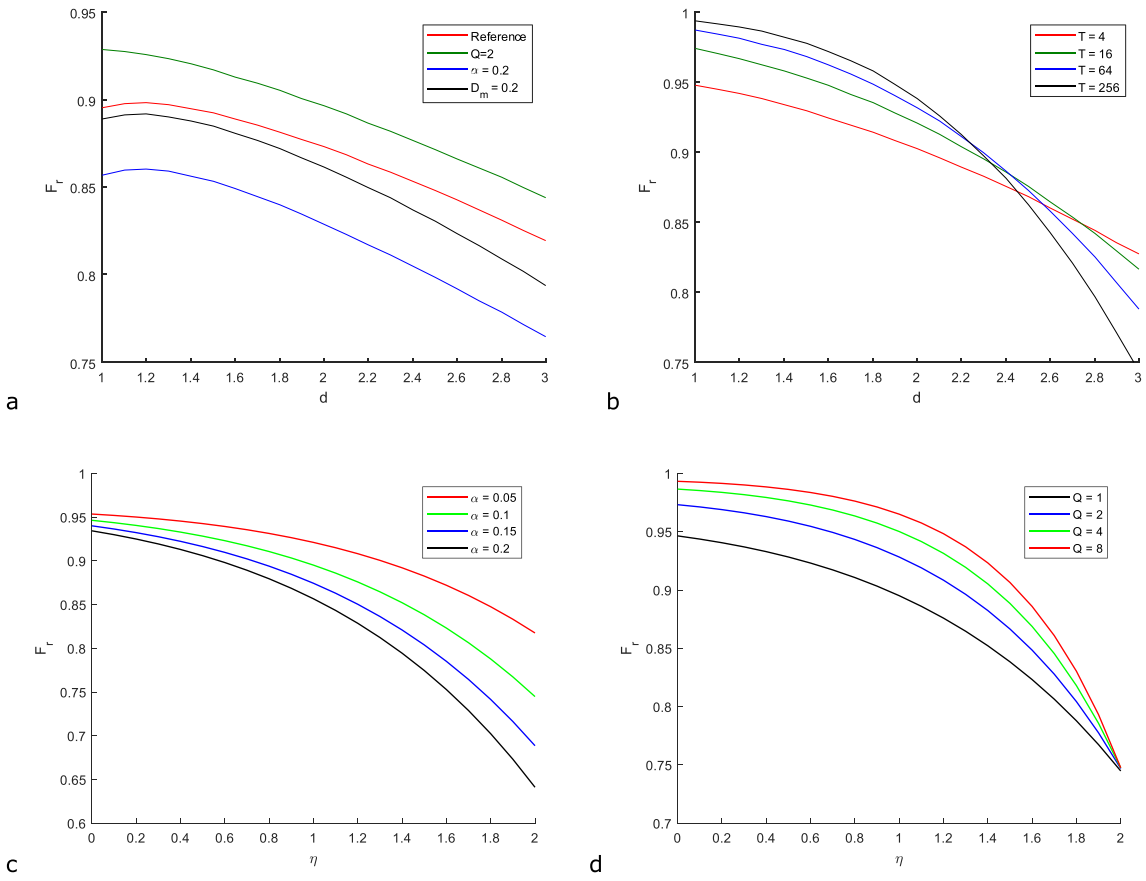

Fig. 8. Recovery as a function of d when (a) Q, α, D_m is varied, and (b) T is varied. Recovery as a function of η, when (c) α is varied, and (d) Q is varied. Unless otherwise specified, $\eta = 1$, $d = 1$, $T = 1$, $Q = 1$, $\alpha = 0.1$, $D_m = 0.1$.

4.7. Generalizations

Since all derived expressions (i.e. F_r, S_T, G) can be written as functions of d, the preceding analyses can be generalized to non-integer dimensions. Non-integer dimensions are primarily used to describe porous media with fractal pore-scale geometry. Dispersive transport in fractal geometry is a distinct aspect of research into pore-scale connectivity and percolation (Bouchaud and Georges, 1990), fractured porous media (Sahimi, 2011), and multi-phase transport (Hunt et al., 2014). Fig. 8a shows that if all other parameters are kept constant, the recovery efficiency mostly decreases monotonically as dimensionality increases. Interestingly however, in the range of small d and small Q, $F_r(d)$ is non-monotonic, with a maximum. Whether this non-monotonicity, and non-integer dimensional radial flow in general, describe meaningful physical phenomena, or are mathematical artefacts, remains to be investigated. Fig. 8b shows that curves of $F_r(d)$ for different T intersect at some point at $d > 2$. This implies that $F_r(T)$ can be non-monotonic in any $d > 2$; amongst all model parameters, such behavior is unique to T. In Section 4.2, we discussed $d = 3$, a specific instance of this.

Analyses under other definitions of hydrodynamic dispersion are also possible, using the methods we have presented. For example, power-law mechanical dispersion $\alpha|v^\eta|$, with $0 \leq \eta \leq 2$ not necessarily an integer. Molecular diffusion corresponds to $\eta = 0$, and standard mechanical dispersion to $\eta = 1$. Other suggested values of η include η 1.2 for Peclet numbers $5 < Pe < 300$ (Sahimi, 1993), η 1.25 when large spatial variances exist in the pore-scale velocity field, (Salles et al., 1993), and $\eta = 2$ in media with solute particle traps (Bouchaud and Georges, 1990), Taylor dispersion (Taylor, 1953), or large tortuosities or low saturations (de Gennes, 1983). Salles et al (1993) also found that η varies continuously with porosity.

The generalized radially axisymmetric ADE for $D = D_m + \alpha|v^\eta|$ is (see Appendix A for derivation)

$$\frac{\partial c}{\partial t} = D(r)\frac{\partial^2 c}{\partial r^2} + \left[\frac{(d-1)}{r}[D_m - (\eta-1)\alpha v^\eta] - v(r)\right]\frac{\partial c}{\partial r}. \tag{37}$$

Then, applying the same steps as in Section 3 and Section 4.1, with $\omega = \int_0^r \frac{v^\eta(r) + D_m/\alpha}{v^3(r)} dr$, results in

$$c(r,t) = \frac{1}{2}c_0 \mathrm{erfc}\left[\frac{(r^d - (dA_d t))}{\sqrt{4d^2\alpha(dA_d t)^{\frac{2d-1}{d}}}}\sqrt{\frac{(3d-2)(3d-2+\eta-\eta d)\alpha A_d}{(3d-2)\alpha A_d^\eta (dA_d t)^{\frac{\eta+d-1-\eta d}{d}} + (3d-2+\eta-\eta d)D_m (dA_d t)^{\frac{d-1}{d}}}}\right] \tag{38}$$

If $\eta = 2, D_m = 0$ is substituted into (38), the solutions for $c(r,t)$ in 1D, 2D and 3D found by Philip (1994) are recovered (see Table 2), with two differences. Philip's exact solutions include an additional term that vanishes for large Q or t, and Philip imposed Robin boundary conditions at the well, whereas we use Dirichlet boundary conditions. Differences

in outcomes originating from different boundary conditions also vanish rapidly as t (Philip, 1994; Chen, 1987) or Q (Aichi and Akitaya, 2018) increases.

The generalized exponents in the geometric dispersion factor $G = Q^x T^y$ are

$$x = [\eta - 2]\left(\frac{1}{2d}\right), \tag{39}$$

$$y = \frac{(d-1)[1-\eta]-1}{2d}. \tag{40}$$

Full expansions of $F_r(\eta = 2)$ and $F_r(d, \eta)$ and the corresponding kinetic dispersion factors, derived from (38) in the same manner as in Sections 4.1 and 4.2, are available in Table 3. Fig. 8c and d illustrate the behavior of $F_r(\eta)$ when α and Q respectively are varied. Remarkably, when $\eta = 2$ and $D = \alpha|v^\eta|$, $1 - F_r \propto T^{-1/2}$ regardless of spatial dimensionality, and recovery is independent of the injection rate. Comparing (39) and (40) reveals an additional limitation of the area-to-volume ratio: F_r is a function of A/V (i.e. $x = y$) only when $D = \alpha|v|$, and never for $D = \alpha|v^\eta|$ with any $\eta \neq 1$. Furthermore, when $D = \alpha|v^\eta|$ with $d = \frac{2-\eta}{1-\eta}$, then $1 - F_r \propto Q^{\frac{\eta-2}{2d}}$, and recovery is independent of the injection period. In Section 4.2, we discussed a specific instance of this, namely $d = 2, \eta = 0$.

5. Discussion

Our more general results agree with specific scenarios discussed in the literature. Several numerical studies (e.g. Bakker, 2010; Lu et al., 2011; Chen, 2014; Barker et al., 2016; Majumdar et al., 2021) showed that in 2D and with $D_m = 0$, the recovery efficiency can be increased by increasing the injection period, or the injection rate, which agrees with the exponents we found for the geometric dispersion factor G. The fact that the recovery efficiency increases as Q or T increases for $d = 2$ has also been observed in practice (e.g. Bloemendal and Hartog, 2018; Kastner et al., 2017). Bakker (2010) modelled an ASR system in a 2D cylindrical flow field in a homogeneous medium, and investigated how varying the injection and storage duration affected the recovery efficiency of freshwater. They demonstrated that the recovery efficiency increases sub-linearly with the number of cycles. The sub-linear increase of the recovery efficiency with cycle number was also observed in practice (Bakr et al., 2013; Kastner et al., 2017) and in other numerical studies (Sommer et al., 2013; Zeghici et al., 2015; Lu et al., 2011; Majumdar et al., 2021). These findings in the literature agree with the bounds we derived for the cycle exponent, $\frac{1}{2} \leq z \leq 1$.

It is possible for a single well to function both as an ATES (heat storage) and ASR (freshwater storage in a brackish aquifer) system simultaneously (Miotliński and Dillon, 2015). Given that, as previously elaborated, heat spreading is primarily controlled by thermal conduction while solute spreading depends mostly on mechanical dispersion, the optimal operational parameters of the well for recovering heat and solutes will differ. When spreading occurs in three dimensions, increasing T might increase the recovery efficiency of freshwater, but decrease that of heat. Therefore, it is impossible to optimize for the recovery efficiency for both heat and solutes simultaneously.

Single well push–pull tracer tests are often used to determine various hydrogeological properties of aquifers, such as porosity (Hall et al., 1991), in-situ microbial activity (Istok et al., 1997), fracture geometry (Klepikova et al., 2016), and geochemical reaction rates (Haggerty et al., 1998), by interpreting breakthrough data at the well during the extraction phase (Schroth et al., 2000). Eqs. (33) and (35) may be used to interpret data from push-pull tests using the methodology of Schroth and Istok (2005). Schroth and Istok's results pertain only to solute transport in 2D and 3D radial flow fields with a more limited model of dispersion, defined as $D = \alpha|v|$, whereas our results apply to a wider range of dispersion models, and also in the presence of multiple coexisting dispersion mechanisms (e.g. $D = D_m + \alpha|v|$).

In this study, to enable an analytical approach, we omitted several aspects. These include heterogeneity in aquifer physical properties, background regional flow, diffusion of heat and solute into confining layers, density driven convection. Nevertheless, these omissions do not negatively affect the ability of simple approximate analyses like that discussed in this study from accurately predicting the behavior of well-aquifer systems under a wide range of realistic conditions (Pophillat et al., 2020a). The assumption of homogeneity has been found to be appropriate for aquifers where the log-conductivity field is autocorrelated and has a variance smaller than 0.25 (Wang et al., 2018). In some systems, the injection and extraction regimes are separated by a stand still storage phase, thus some adaptation may be needed if the velocity-independent component of hydrodynamic dispersion is significant and if the storage phase is long. With low or no regional groundwater flow, the storage period reduces the recovery efficiency by only around 0.5 percentage points per month (Majumdar et al., 2021), and thus has minimal impact. All of these omitted factors would cause a decrease in the recovery efficiency, if they were accounted for. Therefore, our analysis forms a theoretical upper bound of the recovery efficiency of some real applications.

Witt et al (2021) presented injection-extraction experiments of density driven flow with several fully-penetrating and partially-penetrating well configurations, where freshwater was injected into a laboratory-scale brackish aquifer. Experimentally, doubling the injection-extraction rate and halving the injection-extraction duration (maintaining the total volume) led to an increase in recovery efficiency. For three well shapes that create 2D radial flow fields, the recovery efficiency increases they observed were from 0.39 to 0.55, 0.40 to 0.61, and 0.55 to 0.69. They calibrated the hydrogeological parameters based on experimental data, yielding $D_m = 8.8 \cdot 10^{-8}\ m/min$ and $\alpha = 7 \cdot 10^{-3}\ m$. With injection rates around $2 \cdot 10^{-6}\ m^3/min$ to $5 \cdot 10^{-6} m^3/min$, and injection durations of around 60 min, we obtain $S_T = 28$. This value suggests that mechanical dispersion dominates over molecular diffusion. However, they also noted that density driven convection dominated over hydrodynamic mixing in the transport of the salinity gradient. Hence the effect of hydrodynamic dispersion was weaker than that of density driven convection. When we insert their hydrogeological parameters into our equation (26), and set $x = -1/2$, $y = 0$ to account for velocity-independent spreading in 2D, the calculated increases in recovery efficiency would be from 0.39 to 0.57, 0.40 to 0.58, and 0.55 to 0.69, which agrees almost exactly with their experimental results. Our power-law relationship between number of cycles and recovery efficiency also agrees well with their results, which show diminishing marginal returns as the number of cycles increases (compare out Fig. 3 with Witt et al's Figure 9). The agreement between our results for spreading under molecular diffusion, and their results for density driven convection, suggests that the effects of density driven convection on recovery efficiencies, might be similar to the effects of molecular diffusion in some idealized problems. This is possibly because density driven convection is a form of velocity-independent spreading (at these low viscosities) that results in a radial plume shape (i.e. conical shape, see Witt et al's Fig. 2h).

The modelled flow field geometries often arise as small or large time limiting cases in other flow field geometries. For example, a point source in a typical vertically confined aquifer generates a 3D spherical solute plume at small times, and a 2D spherical solute plume (i.e. cylindrical) at large times when the size of the plume has grown large (e.g. Schroth and Istok, 2005). From field data, Bloemendal and Hartog (2018) found that when the outlet screen height of a fully penetrating well in a confined aquifer is reduced, the recovery efficiency of heat decreases. This is because the flow field of a non-fully-penetrating well is three-dimensional at small times, and that losses are larger when spatial dimensionality d increases (see Eq. (21)). For space-use efficiency, often multiple wells are spatially distributed in a single large aquifer, such as

with zonation patterns (e.g. Sommer et al., 2015). In such implementations, the dimensionality of the flow field essentially depends on whether the neighboring wells mutually interfere (Kandelous et al., 2011), thus a transitional time scale also exists for such systems.

During transitional regimes when solute plumes transition from, for example, a 3D to 2D geometry, the dispersive behavior is bounded by the solutions for 2D and 3D systems. This is because the radial velocity of the plume front, which affects the plume size, surface area, and mechanical dispersion, is bounded from above by the 2D solution, and from below by the 3D solution. Consequently, it appears plausible that a mathematical description of dispersion and recovery during transitional times can be obtained by setting $2 < d < 3$ in the analysis (see Section 4.7), and is a topic for further research. If and only if $d > 2$, the recovery efficiency varies non-monotonically with well parameters, and retardation may increase the recovery efficiency instead of decreasing it. Hence, systems that undergo transitional regimes experience profound differences in parameter sensitivity across the small, transitional, and large time scales.

6. Conclusions

In our analysis, we approximated solute and heat transport, towards the recovery efficiency of injected solute and heat in 1D, 2D, and 3D homogeneous aquifers under cyclic radial flow. These new analytical solutions are broadly applicable in sensitivity analyses, as they comprise simple closed-form expressions. These expressions enable to determine the effect on the recovery efficiency of varying the: (i) mechanical dispersion and diffusion parameters, (ii) aquifer hydrogeological parameters, (iii) injection and extraction duration, (iv) injection and extraction rate, (v) flow field geometry, (vi) number of operating cycles and (vii) extraction volume relative to injection volume. Hence, a first-order assessment of aquifer-well systems can be conducted with minimal computational demand, e.g. to pave the way for further focussed evaluations with numerical modelling or exact analyses, by enabling the identification of interesting regions in parameter space. As discussed, our solutions are in broad agreement with various analytical, experimental, and numerical modelling studies in the literature.

Key factors that determine the recovery efficiency are the flow field geometry, and whether mechanical dispersion or diffusion dominates. Whereas in 1D and 2D flow fields, recovery efficiency is a non-decreasing function of the injection-extraction duration and rate, in 3D flow fields, it increases with the duration of the cycle when velocity-dependent mechanical dispersion dominates, but decreases if velocity-independent diffusion dominates. Consequently, if velocity-dependent and independent dispersion are of comparable magnitude in 3D spreading, recovery varies with cycle duration non-monotonically, peaking at a maximum. Therefore, as solute and heat injection/extraction are dominated by different dispersion processes, it may be impossible to optimize for the recovery efficiency of both simultaneously. Another consequence is that when diffusion dominates over mechanical dispersion, chemical or thermal retardation leads to decreased recovery in 1D and 2D flow fields, but increased recovery in 3D flow fields. We generalized this to non-integer dimensional flow fields, and for mechanical dispersion processes that have an arbitrary power-law dependence on advection velocity.

As the sensitivity of the recovery efficiency to parameters is highly dependent on the dominant dispersion process, we introduce the kinetic dispersion factor, for identifying the dominant dispersion process. We also introduce the geometric dispersion factor, a simplified form of our full solution for recovery efficiency, that applies if the spreading of solutes or heat may be described by a single dispersion process. We show that the classical Area-to-Volume ratio is a special case of the geometric dispersion factor that characterizes the recovery efficiency only in the specific scenario where mechanical dispersion with linear velocity dependence is the sole mechanism of spreading.

CRediT authorship contribution statement

D.W.S. Tang: Conceptualization, Methodology, Software, Validation, Formal analysis, Investigation, Writing - original draft, Writing – review & editing. **S.E.A.T.M. Zee:** Writing - review & editing, Supervision, Project administration, Funding acquisition.

Declaration of Competing Interest

The authors declare that they have no known competing financial interests or personal relationships that could have appeared to influence the work reported in this paper.

Acknowledgements

This research was conducted in the context of the project "*Re-USe of Treated effluent for agriculture RUST*" of the Closed Cycles program and was funded by the Netherlands Organization for Scientific Research under contract NWOGK.2016.016. We thank Anton Leijnse (Wageningen University) and Ruud Bartholomeus (KWR Water Research Institute) for helpful discussions, and Hennie Gertsen (Wageningen University) for making Fig. 1.

Appendix A. Derivation of the Advection-Dispersion Equation for nonlinear mechanical dispersion

To derive the ADE for the generalized power-law dispersion case $D(r) = D_m + \alpha v^{\eta}(r)$, we begin from a modified form of Eqs. (3) and (4) of Gelhar and Collins (1971):

$$\frac{\partial c}{\partial t} + v\frac{\partial c}{\partial r} = \frac{\alpha}{h_2 h_3}\frac{\partial}{\partial r}\left[h_2 h_3 v^{\eta}\frac{\partial c}{\partial r}\right] + \frac{D_m}{h_2 h_3}\frac{\partial}{\partial r}\left[h_2 h_3 \frac{\partial c}{\partial r}\right], \tag{A1}$$

$$\frac{1}{h_2 h_3}\frac{\partial}{\partial r}[h_2 h_3 v] = 0, \tag{A2}$$

where h_2 and h_3 are scale factors of the curvilinear coordinates orthogonal to the primary coordinate r, and the condition (A2) implies the incompressibility of water.

Rewriting (A1) in the following form

$$\frac{\partial c}{\partial t} + v\frac{\partial c}{\partial r} = \frac{\alpha}{h_2 h_3}\frac{\partial}{\partial r}\left[h_2 h_3 v v^{\eta-1}\frac{\partial c}{\partial r}\right] + \frac{D_m}{h_2 h_3}\frac{\partial}{\partial r}\left[h_2 h_3 v \frac{1}{v}\frac{\partial c}{\partial r}\right] \tag{A3}$$

and substituting (A2) into (A3) yields

$$\frac{\partial c}{\partial t}+v\frac{\partial c}{\partial r}=\alpha v\frac{\partial}{\partial r}\left[v^{\eta-1}\frac{\partial c}{\partial r}\right]+D_m v\frac{\partial}{\partial r}\left[\frac{1}{v}\frac{\partial c}{\partial r}\right], \tag{A4}$$

which can be fully expanded to

$$\frac{\partial c}{\partial t}+v\frac{\partial c}{\partial r}=\alpha(\eta-1)v\frac{\partial c}{\partial r}\frac{\partial v}{\partial r}v^{\eta-2}+\alpha v^{\eta}\frac{\partial^2 c}{\partial r^2}+D_m v\left[\frac{1}{v}\frac{\partial^2 c}{\partial r^2}-\frac{1}{v^2}\frac{\partial v}{\partial r}\frac{\partial c}{\partial r}\right], \tag{A5}$$

Substituting the following into (A5) (see Section 3),

$$v(r,d)=\frac{A_d}{r^{d-1}},$$

$$\frac{\partial v}{\partial r}=(1-d)\frac{A_d}{r^d}=(1-d)\frac{v}{r},$$

yields the general ADE (37):

$$\frac{\partial c}{\partial t}=D(r)\frac{\partial^2 c}{\partial r^2}+\left[\frac{(d-1)}{r}\left[D_m-(\eta-1)\alpha v^{\eta}\right]-v(r)\right]\frac{\partial c}{\partial r}. \tag{A6}$$

Setting $\eta=1$ recovers the specific case described in (5), where $D(r)=D_m+\alpha v(r)$.

References

Aichi, M., Akitaya, K., 2018. Analytical solution for a radial advection-dispersion equation including both mechanical dispersion and molecular diffusion for a steady-state flow field in a horizontal aquifer caused by a constant rate injection from a well. Hydrol. Res. Lett. 12 (3), 23–27.

Anderson, M.P., 1984. Movement of contaminants in groundwater: groundwater transport–advection and dispersion. Groundwater Contam. 37–45.

Anderson, M.P., 2005. Heat as a ground water tracer. Groundwater 43 (6), 951–968.

Bakker, M., 2010. Radial Dupuit interface flow to assess the aquifer storage and recovery potential of saltwater aquifers. Hydrogeol. J. 18 (1), 107–115.

Bakr, M., van Oostrom, N., Sommer, W., 2013. Efficiency of and interference among multiple Aquifer Thermal Energy Storage systems; A Dutch case study. Renewable Energy 60, 53–62.

Barker, J.L.B., Hassan, M.M., Sultana, S., Ahmed, K.M., Robinson, C.E., 2016. Numerical evaluation of community-scale aquifer storage, transfer and recovery technology: a case study from coastal Bangladesh. J. Hydrol. 540, 861–872.

Bloemendal, M., Hartog, N., 2018. Analysis of the impact of storage conditions on the thermal recovery efficiency of low-temperature ATES systems. Geothermics 71, 306–319.

Bouchaud, J.-P., Georges, A., 1990. Anomalous diffusion in disordered media: statistical mechanisms, models and physical applications. Phys. Rep. 195 (4-5), 127–293.

Chen, C.-S., 1987. Analytical solutions for radial dispersion with Cauchy boundary at injection well. Water Resour. Res. 23 (7), 1217–1224.

Chen, Y., 2014. Aquifer storage and recovery in saline aquifers. Doctoral dissertation. Georgia Institute of Technology.

Cirkel, D.G., van der Zee, S.E.A.T.M., Meeussen, J.C.L., 2015. Front spreading with nonlinear sorption for oscillating flow. Water Resour. Res. 51 (4), 2986–2993.

Doughty, C., Hellström, G., Tsang, C.F., Claesson, J., 1982. A dimensionless parameter approach to the thermal behavior of an aquifer thermal energy storage system. Water Resour. Res. 18 (3), 571–587.

De Gennes, P.G., 1983. Hydrodynamic dispersion in unsaturated porous media. J. Fluid Mech. 136 (-1), 189. https://doi.org/10.1017/S0022112083002116.

Dey, B., Sekhar, G.R., 2014. Mass transfer and species separation due to oscillatory flow in a Brinkman medium. Int. J. Eng. Sci. 74, 35–54.

Drijver, B., van Aarssen, M., Zwart, B.D., 2012. High-temperature aquifer thermal energy storage (HT-ATES): sustainable and multi-usable. In: Proceedings of the Innostock, pp. 1–10.

Duffie, J.A., Beckman, W.A., 2013. Solar Engineering of Thermal Processes. John Wiley & Sons.

Eeman, S., De Louw, P.G.B., Van der Zee, S.E.A.T.M., 2017. Cation exchange in a temporally fluctuating thin freshwater lens on top of saline groundwater. Hydrogeol. J. 25 (1), 223–241.

Forkel, C., Daniels, H., 1995. Finite element simulation of circulation in large scale thermal energy storage basins. Adv. Water Resour. 18 (3), 147–158.

Gelhar, L.W., Collins, M.A., 1971. General analysis of longitudinal dispersion in nonuniform flow. Water Resour. Res. 7 (6), 1511–1521.

Gouze, P., Le Borgne, T., Leprovost, R., Lods, G., Poidras, T., Pezard, P., 2008. Non-Fickian dispersion in porous media: 1. Multiscale measurements using single-well injection withdrawal tracer tests. Water Resour. Res. 44 (6).

Guimerà, J., Ortuño, F., Ruiz, E., Delos, A., Pérez-Paricio, A., 2007. Influence of ground-source heat pumps on groundwater. Conference Proceedings: European Geothermal Congress.

Haggerty, R., Schroth, M.H., Istok, J.D., 1998. Simplified method of "push-pull" test data analysis for determining in situ reaction rate coefficients. Groundwater 36 (2), 314–324.

Hall, S.H., Luttrell, S.P., Cronin, W.E., 1991. A method for estimating effective porosity and ground-water velocity. Groundwater 29 (2), 171–174.

Harbaugh, A.W., 2005. In: MODFLOW-2005, The US Geological Survey Modular Ground-water Model: The Ground-water Flow Process. US Department of the Interior, US Geological Survey, Reston, VA, pp. 6–A16.

Hoopes, J.A., Harleman, D.R.F., 1967. Dispersion in radial flow from a recharge well. J. Geophys. Res. 72 (14), 3595–3607.

Hunt, A., Ewing, R., Ghanbarian, B., 2014. Percolation Theory for Flow in Porous Media. Springer.

Istok, J.D., Humphrey, M.D., Schroth, M.H., Hyman, M.R., O'Reilly, K.T., 1997. Single-well, "push-pull" test for in situ determination of microbial activities. Groundwater 35 (4), 619–631.

Kandelous, M.M., Šimůnek, J., van Genuchten, M.T., Malek, K., 2011. Soil water content distributions between two emitters of a subsurface drip irrigation system. Soil Sci. Soc. Am. J. 75 (2), 488–497.

Kastner, O., Norden, B., Klapperer, S., Park, S., Urpi, L., Cacace, M., Blöcher, G., 2017. Thermal solar energy storage in Jurassic aquifers in Northeastern Germany: a simulation study. Renewable Energy 104, 290–306.

Kim, J., Lee, Y., Yoon, W.S., Jeon, J.S., Koo, M.-H., Keehm, Y., 2010. Numerical modeling of aquifer thermal energy storage system. Energy 35 (12), 4955–4965.

Klepikova, M.V., Le Borgne, T., Bour, O., Dentz, M., Hochreutener, R., Lavenant, N., 2016. Heat as a tracer for understanding transport processes in fractured media: Theory and field assessment from multiscale thermal push-pull tracer tests. Water Resour. Res. 52 (7), 5442–5457.

Laemmel, T., Mohr, M., Schack-Kirchner, H., Schindler, D., Maier, M., 2019. 1D air pressure fluctuations cannot fully explain the natural pressure-pumping effect on soil gas transport. Soil Sci. Soc. Am. J. 83 (4), 1044–1053.

Langevin, C.D., Guo, W., 2006. MODFLOW/MT3DMS–based simulation of variable-density ground water flow and transport. Groundwater 44 (3), 339–351.

Lee, T.C., 1998. Applied Mathematics in Hydrogeology. Routledge.

Lee, K.S., 2010. A review on concepts, applications, and models of aquifer thermal energy storage systems. Energies 3 (6), 1320–1334.

Lin, Y.-C., Hu, T.-F., Yeh, H.-D., 2019. Analytical model for heat transfer accounting for both conduction and dispersion in aquifers with a Robin-type boundary condition at the injection well. Water Resour. Res. 55 (8), 7379–7399.

Lowry, C.S., Anderson, M.P., 2006. An assessment of aquifer storage recovery using ground water flow models. Groundwater 44 (5), 661–667.

Lu, C., Du, P., Chen, Y., Luo, J., 2011. Recovery efficiency of aquifer storage and recovery (ASR) with mass transfer limitation. Water Resour. Res. 47 (8) https://doi.org/10.1029/2011WR010605.

Majumdar, S., Miller, G.R., Sheng, Z., 2021. Optimizing multiwell aquifer storage and recovery systems for energy use and recovery efficiency. Groundwater.

Miotliński, K., Dillon, P.J., 2015. Relative recovery of thermal energy and fresh water in aquifer storage and recovery systems. Groundwater 53 (6), 877–884.

Molinari, J., Peaudeceff, P., 1977. Essais conjoints en laboratoire et sur le terrain en rue d'une approach simplefi6e de la pr6vision des propagations de substances miscibles dans les aquif•res r6els, paper presented at Symposium on Hydrodynamic Diffusion and Dispersion in Porous Media. Int. Assoc. for Hydraul. Res., Pavis, Italy.

Narain-Ford, D., Bartholomeus, R., Raterman, B., van Zaanen, I., ter Laak, T., van Wezel, A.P., Dekker, S.C., 2020. Shifting the imbalance: Intentional reuse of Dutch sewage effluent in sub-surface irrigation. Sci. Total Environ. 142214.

Nilson, R.H., Peterson, E.W., Lie, K.H., Burkhard, N.R., Hearst, J.R., 1991. Atmospheric pumping: a mechanism causing vertical transport of contaminated gases through fractured permeable media. J. Geophys. Res. Solid Earth 96 (B13), 21933–21948.

Novo, A.V., Bayon, J.R., Castro-Fresno, D., Rodriguez-Hernandez, J., 2010. Review of seasonal heat storage in large basins: water tanks and gravel–water pits. Appl. Energy 87 (2), 390–397.

Pauw, P.S., van der Zee, S.E.A.T.M., Leijnse, A., Oude Essink, G.H.P., 2016. Saltwater upconing due to cyclic pumping by horizontal wells in freshwater lenses. Groundwater 54 (4), 521–531.

Penny, G.S., Conway, M.W., Briscoe, J.E., 1983. Enhanced load water-recovery technique improves stimulation results. SPE Annual Technical Conference and Exhibition. Society of Petroleum Engineers.
Philip, J.R., 1994. Some exact solutions of convection-diffusion and diffusion equations. Water Resour. Res. 30 (12), 3545–3551.
Pool, M., Dentz, M., Post, V.E.A., 2016. Transient forcing effects on mixing of two fluids for a stable stratification. Water Resour. Res. 52 (9), 7178–7197.
Pophillat, W., Attard, G., Bayer, P., Hecht-Méndez, J., Blum, P., 2020a. Analytical solutions for predicting thermal plumes of groundwater heat pump systems. Renewable Energy 147, 2696–2707.
Pophillat, W., Bayer, P., Teyssier, E., Blum, P., Attard, G., 2020b. Impact of groundwater heat pump systems on subsurface temperature under variable advection, conduction and dispersion. Geothermics 83, 101721.
Salles, J., Thovert, J.-F., Delannay, R., Prevors, L., Auriault, J.-L., Adler, P.M., 1993. Taylor dispersion in porous media. Determination of the dispersion tensor. Phys. Fluids A Fluid Dyn. 5 (10), 2348–2376.
Sahimi, M., 2011. Flow and Transport in Porous Media and Fractured Rock: From Classical Methods to Modern Approaches. John Wiley & Sons.
Sahimi, M., 1993. Flow phenomena in rocks: from continuum models to fractals, percolation, cellular automata, and simulated annealing. Rev. Mod. Phys. 65 (4), 1393–1534.
Sauty, J.P., 1977. Contribution b. l'identification des parameters de dispersion dans les aquif•res par interpr6tation des exp6riences de tracage. dissertation. Univ. Sci. et Med. et Inst. Natl. Polytech. de Grenoble, Grenoble, France.
Sauty, J.P., Gringarten, A.C., Menjoz, A., Landel, P.A., 1982. Sensible energy storage in aquifers: 1. Theoretical study. Water Resour. Res. 18 (2), 245–252.
Sanz-Prat, A., Lu, C., Finkel, M., Cirpka, O.A., 2016. Using travel times to simulate multi-dimensional bioreactive transport in time-periodic flows. J. Contam. Hydrol. 187, 1–17.
Schout, G., Drijver, B., Gutierrez-Neri, M., Schotting, R., 2014. Analysis of recovery efficiency in high-temperature aquifer thermal energy storage: a Rayleigh-based method. Hydrogeol. J. 22 (1), 281–291.
Schout, G., Drijver, B., Schotting, R.J., 2016. The influence of the injection temperature on the recovery efficiency of high temperature aquifer thermal energy storage: Comment on Jeon et al., 2015. Energy 103, 107–109.
Schroth, M.H., Istok, J.D., Haggerty, R., 2000. In situ evaluation of solute retardation using single-well push–pull tests. Adv. Water Resour. 24 (1), 105–117.
Schroth, M.H., Istok, J.D., 2005. Approximate solution for solute transport during spherical-flow push-pull tests. Groundwater 43 (2), 280–284.
Scotter, D.R., Raats, P.A.C., 1968. Dispersion in porous mediums due to oscillating flow. Water Resour. Res. 4 (6), 1201–1206.
Shi, W., Wang, Q., Zhan, H., 2020. New simplified models of single-well push-pull tests with mixing effect. Water Resour. Res. 56 (8) e2019WR026802.
Sommer, W., Valstar, J., van Gaans, P., Grotenhuis, T., Rijnaarts, H., 2013. The impact of aquifer heterogeneity on the performance of aquifer thermal energy storage. Water Resour. Res. 49 (12), 8128–8138.
Sommer, W., Valstar, J., Leusbrock, I., Grotenhuis, T., Rijnaarts, H., 2015. Optimization and spatial pattern of large-scale aquifer thermal energy storage. Appl. Energy 137, 322–337.
Stauffer, P.H., Rahn, T., Ortiz, J.P., Salazar, L.J., Boukhalfa, H., Behar, H.R., Snyder, E.E., 2019. Evidence for high rates of gas transport in the deep subsurface. Geophys. Res. Lett. 46 (7), 3773–3780.
Taylor, G.I., 1953. Dispersion of soluble matter in solvent flowing slowly through a tube. Proc. R. Soc. London. Ser. A. Math. Phys. Sci. 219 (1137), 186–203.
Vandenbohede, A., Louwyck, A., Lebbe, L., 2009. Conservative solute versus heat transport in porous media during push-pull tests. Transp. Porous Media 76 (2), 265–287.
Vandenbohede, A., Hermans, T., Nguyen, F., Lebbe, L., 2011. Shallow heat injection and storage experiment: heat transport simulation and sensitivity analysis. J. Hydrol. 409 (1-2), 262–272.
van de Craats, D., van der Zee, S.E.A.T.M., Sui, C., Asten, P.J.A., Cornelissen, P., Leijnse, A., 2020. Soil sodicity originating from marginal groundwater. Vadose Zone J. 19 (1) https://doi.org/10.1002/vzj2.v19.110.1002/vzj2.20010.
van der Zee, S.E.A.T.M., Shah, S.H.H., Vervoort, R.W., 2014. Root zone salinity and sodicity under seasonal rainfall due to feedback of decreasing hydraulic conductivity. Water Resour. Res. 50 (12), 9432–9446.
van Dijke, M.I.J., van der Zee, S.E.A.T.M., 1998. Modeling of air sparging in a layered soil: numerical and analytical approximations. Water Resour. Res. 34 (3), 341–353.
van Duijn, C.J., van der Zee, S.E.A.T.M., 2018. Large time behaviour of oscillatory nonlinear solute transport in porous media. Chem. Eng. Sci. 183, 86–94.
van Halem, D., Vet, W.d., Verberk, J., Amy, G., van Dijk, H., 2011. Characterization of accumulated precipitates during subsurface iron removal. Appl. Geochem. 26 (1), 116–124.
van Lopik, J.H., Hartog, N., Zaadnoordijk, W.J., 2016. The use of salinity contrast for density difference compensation to improve the thermal recovery efficiency in high-temperature aquifer thermal energy storage systems. Hydrogeol. J. 24 (5), 1255–1271.
Veling, E.J.M., 2012. Radial transport in a porous medium with Dirichlet, Neumann and Robin-type inhomogeneous boundary values and general initial data: analytical solution and evaluation. J. Eng. Math. 75 (1), 173–189.
Wang, P., Chen, G.Q., 2015. Environmental dispersion in a tidal wetland with sorption by vegetation. Commun. Nonlinear Sci. Numer. Simul. 22 (1-3), 348–366.
Wang, Q., Shi, W., Zhan, H., Gu, H., Chen, K., 2018. Models of single-well push-pull test with mixing effect in the wellbore. Water Resour. Res. 54 (12), 10–155.
Witt, L., Müller, M.J., Gröschke, M., Post, V.E., 2021. Experimental observations of aquifer storage and recovery in brackish aquifers using multiple partially penetrating wells. Hydrogeol. J. 1–16.
Woess, W., 2000. Random Walks on Infinite Graphs and Groups. Cambridge University Press.
Yang, S.Y., Yeh, H.D., Li, K.Y., 2010. Modelling transient temperature distribution for injecting hot water through a well to an aquifer thermal energy storage system. Geophys. J. Int. 183 (1), 237–251.
Yates, S.R., 1990. An analytical solution for one-dimensional transport in heterogeneous porous media. Water Resour. Res. 26 (10), 2331–2338.
Zeghici, R.M., Oude Essink, G.H.P., Hartog, N., Sommer, W., 2015. Integrated assessment of variable density–viscosity groundwater flow for a high temperature mono-well aquifer thermal energy storage (HT-ATES) system in a geothermal reservoir. Geothermics 55, 58–68.